



Title	Studies on Preparation and Characterization of Ultrafine Particles of Rare Earth-Based Oxide
Author(s)	Masui, Toshiyuki
Citation	大阪大学, 1998, 博士論文
Version Type	VoR
URL	https://doi.org/10.11501/3143988
rights	
Note	

Osaka University Knowledge Archive : OUKA

<https://ir.library.osaka-u.ac.jp/>

Osaka University

甲6405

**Studies on Synthesis and Characterization of Ultrafine
Particles of Rare Earth-Based Oxide**

(希土類系酸化物超微粒子の合成とそのキャラクタリゼーションに関する研究)

1998

Toshiyuki Masui

Department of Applied Chemistry
Faculty of Engineering
Osaka University

**Studies on Synthesis and Characterization of Ultrafine
Particles of Rare Earth-Based Oxide**

(希土類系酸化物超微粒子の合成とそのキャラクタリゼーションに関する研究)

1998

Toshiyuki Masui

Department of Applied Chemistry

Faculty of Engineering

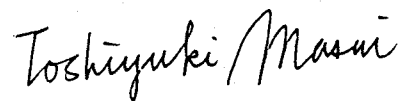
Osaka University

Preface

The work on this thesis has been carried out under the guidance of Professor Dr. Gin-ya Adachi at Department of Applied Chemistry, Faculty of Engineering, Osaka University.

The objects of this thesis are to synthesize and characterize the nanometer-size rare earth-based oxide especially cerium containing oxide, and to investigate their potential for the application as new promoter in the automotive exhaust three-way catalysts.

The author wishes that the findings obtained in this work provide useful information and suggestion for further development of the chemistry on the rare earth-based oxide nanoparticles and for establishment of their applications in the 21 century.



Toshiyuki Masui

Department of Applied Chemistry

Faculty of Engineering

Osaka University

Yamadaoka 2-1, Suita, Osaka 565

Japan

January 1998

Contents

<i>General Introduction</i>	1
<i>List of Publications</i>	4

Chapter 1

Characterization of Cerium(IV) Oxide Ultrafine Particles Prepared Using Thermal Relaxation Process of Polymer Thin Film

1.1. Introduction	5
1.2. Experimental Details	6
1.3. Results and Discussion	8
1.4. Conclusions	14

Chapter 2

Characterization of Cerium(IV) Oxide Ultrafine Particles Prepared Using Reversed Micelles

2.1. Introduction	15
2.2. Experimental Details	17
2.3. Results and Discussion	19
2.4. Conclusions	32

Chapter 3

Characterization and Catalytic Properties of Cerium-Zirconium Oxide Ultrafine Particles Prepared by the Microemulsion Method.

3.1. Introduction	34
3.2. Experimental Details	35
3.3. Results and Discussion	36
3.4. Conclusions	44

Chapter 4

Reduction Behavior of Cerium-Zirconium Oxide Prepared by Means of a New Synthesis Method Using Thermal Decomposition of Cerium Zirconyl Oxalate

4.1. Introduction	46
4.2. Experimental Details	47
4.3. Results and Discussion	49
4.4. Conclusions	54

<i>Summary</i>	55
-----------------------	----

<i>References</i>	57
--------------------------	----

<i>Acknowledgements</i>	61
--------------------------------	----

General Introduction

In recent years, ultrafine nanometer-sized particles have attracted much attention due to the physical and chemical properties which are significantly different from those of bulk materials [1], and the production of ultrafine particles becomes one of the most important subjects of the new technologies. The reduction in size of the materials and components plays an important role in the development of the miniaturization technology, and causes new applications such as catalysts due to the great value of the surface to volume ratio. Therefore, it is very important to have general methods for obtaining ultrafine particles by simple and reproducible methods.

Cerium oxide is one of major compounds in the useful rare earth family and has been applied as one of glass-polishing materials, ultraviolet absorbent, and automotive exhaust promoter. Fine particles of cerium oxide with very small size have great potentiality to become new materials that are useful for more precision polishing, fine UV absorbent, high activity catalyst, and high sinterable ceramics. Many workers have prepared them using various methods such as inert gas condensation of Ce metal (matrix isolation) followed by oxidation with an O₂ gas [2], hydrolysis of cerium isopropoxide (alkoxide process) [3], a process of homogeneous precipitation using urea or hexamethylenetetramine [4], forced hydrolysis of cerium salts in the presence of diluted sulfuric acid [5], hydrothermal synthesis technique [6 - 8], and an electrochemical synthesis [9]. In these references mentioned above, some of the properties such as sinterability of the particles, thermal stability of specific surface area, and catalytic properties also have been investigated.

One of the problems associated with nanometer-sized metal particles is that it is difficult to handle them in air because of their high surface energy. This is the reason why many workers have interest in preparing fine metal particles incorporated in polymer films [10 - 16]. As a work on this line, a new process to prepare composite films which consist of a polymer and ultrafine metal particles was reported [17], and this process was called the relaxative auto-dispersion (RAD) process. In this composite material, nanometer-sized metal particles are stably and uniformly dispersed in the polymer matrix. This process may also be applicable to prepare nm-sized compound particles.

On the other hand, recently the use of reversed micelles to synthesize nanoparticles has been progressed [18]. The reversed micelles formed in a non-polar organic solvent can solubilize several amount of water inside it, and the size of the droplet varies with the amount of water solubilized in the system [19 -21]. They have the ability to exchange the content of their water pools by collision [22 - 25], and it makes possible to react metallic ions with other chemical species solubilized in different micelles [26]. Using this method one can easily synthesize nano-particles because the reaction site is limited inside the reversed micelles and the formed particles was stabilized and protected by the surfactant molecules adsorbed on the surface.

The present work deals with preparation and characterization of ultrafine particles of a rare earth-based oxide, and especially focus on CeO_2 and the $\text{CeO}_2\text{-ZrO}_2$ system which are applied as a promoter in the automotive exhaust three-way catalysts. In addition, a new process using thermal decomposition of cerium-zirconium oxalate is proposed to obtain $\text{CeO}_2\text{-ZrO}_2$ with high performance.

This thesis consists of following four chapters.

In **Chapters 1 and 2**, two kinds of preparation process were employed to obtain the smallest cerium oxide ultrafine particles ever reported. **Chapter 1** describes the preparation of CeO_2 ultrafine particles using thermal relaxation of polymer film, which is called the RAD process. The particles obtained in this process were characterized by high-resolution transmission electron microscope and ultraviolet-visible absorption spectra measurements.

In **Chapter 2**, CeO_2 ultrafine particles were prepared using the reaction within reversed micelles, and a suitable system for the formation of the smallest particles was optimized. The size and morphology of the obtained particles were characterized, and effects of the fine particle size on the optical absorption property and catalytic activity were investigated.

In **Chapter 3**, the preparation method using reversed micelles was expanded to the $\text{CeO}_2\text{-ZrO}_2$ system which has been applied as a promoter in the automotive exhaust three-way catalysts. Effects of calcination temperature on the specific surface area of the particles were examined to estimate the thermal stability of them. Also, their thermal stabilities for catalytic activities were discussed by measuring the CO oxidation activity of the particles supported on alumina and

comparing it with that of conventional co-precipitated catalysts both before and after the calcination at 1273 K in air for 5 h.

Chapter 4 describes a new preparation method for $\text{CeO}_2\text{-ZrO}_2$ powders for a promoter in the automotive exhaust catalysts. Usually the $\text{CeO}_2\text{-ZrO}_2$ powders were synthesized from their hydroxide by the calcination of them in air. In the new method, cerium-zirconium oxalate was employed to obtain high-performance $\text{CeO}_2\text{-ZrO}_2$. The $\text{CeO}_2\text{-ZrO}_2$ powders were synthesized by thermal decomposition of the oxalate in an inert gas flow followed by the calcination at relative low temperature, and the role of the phase, structure, and preparation process in the oxygen release properties was discussed by comparing them with those of conventional samples synthesized from hydroxide.

List of Publications

- [1] Characterization of CeO₂ Ultrafine Particles Prepared Using a Thermal Relaxation Technique
Toshiyuki Masui, Ken-ichi Machida, Takao Sakata, Hirotaro Mori, and Gin-ya Adachi
Chemistry Letters, **1996**, 75-76.
- [2] Preparation and Characterization of Cerium Oxide Ultrafine Particles Dispersed in Polymer Thin Films
Toshiyuki Masui, Ken-ichi Machida, Takao Sakata, Hirotaro Mori, and Gin-ya Adachi
Journal of Alloys and Compounds, **256**, 97-101 (1997).
- [3] Characterization of Cerium(IV) Oxide Ultrafine Particles Prepared Using Reversed Micelles
Toshiyuki Masui, Kazuyasu Fujiwara, Ken-ichi Machida, Takao Sakata, Hirotaro Mori, and Gin-ya Adachi
Chemistry of Materials, **9**, 2197-2204 (1997).
- [4] Carbon Monoxide Oxidation Characteristics over the Al₂O₃-supported CeO₂-ZrO₂ Catalysts Prepared by the Microemulsion Method
Toshiyuki Masui, Kazuyasu Fujiwara, Yumin Peng, Ken-ichi Machida, and Gin-ya Adachi
Chemistry Letters, **1997**, 1285-1286.
- [5] Characterization and Catalytic Properties of CeO₂-ZrO₂ Ultrafine Particles Prepared by the Microemulsion Method
Toshiyuki Masui, Kazuyasu Fujiwara, Yumin Peng, Takao Sakata, Ken-ichi Machida, Hirotaro Mori, and Gin-ya Adachi
Journal of Alloys and Compounds, in preparation.

Chapter 1

Characterization of Cerium(IV) Oxide Ultrafine Particles Prepared Using Thermal Relaxation Process of Polymer Thin Film

1.1. Introduction

As mentioned in General Introduction, ultrafine nanometer-sized particles have attracted much attention since such particles often exhibit the physical and chemical properties that are significantly different from those of bulk materials [1]. However, they are liable to aggregate one another and it is difficult to handle them because they have high surface energy and activity. Therefore, usually, nanometer-sized fine particles have been prepared by incorporating into matrices, e.g., polymer films [10 - 16]. The resulting polymer composite thin films containing metal or compound particles are of interest for basic and technical applications such as optical filters, electrical shielding and protective coatings. While working on this activity, Noguchi and co-workers have found a new process to prepare the composite films that consist of organic polymers and ultrafine metal particles [17]. This process is known as the relaxative auto-dispersion (RAD) process and has been developed for such systems as gold fine particles embedded in polymer matrix [17, 27 -30]. This process may also be applicable to other systems such as the nm-sized compound particles incorporated into the polymer matrix.

In Chapter 1, the RAD process was employed to prepare the smallest nanosize cerium oxide ultrafine particles ever reported, and the size and distribution of the particles obtained in this process were characterized by high-resolution transmission electron microscope observation. Moreover, to identify whether there are some effects based on fine size to the optical property of cerium oxide, ultraviolet-visible absorption spectra were measured using the composite films that the cerium oxide ultrafine particles dispersed in polymer matrices.

1.2. Experimental Details

1.2.1. Preparation of CeO₂ Ultrafine Particles by RAD Process

The vacuum deposition of polymer film matrices was made in a conventional apparatus of glass chamber (20 cm in diameter and 25 cm in height) equipped with an evaporator (tantalum boat) in the lower part. The substrate was mounted on the holder located 5 cm above the evaporator in the center of the chamber. Nylon 11 (Aldrich Chem.) film of 150 nm thickness was usually used in this study as the polymer matrix and was prepared by vapor deposition under a background pressure condition of below 1.33×10^{-3} Pa on a NaCl single crystal fixed on stainless substrate. The film was separated from the NaCl substrate by dissolving it in water and then it was collected on a copper grid covered with an amorphous collodion film which was used as a sample holder for transmission electron microscopy. The grid was fixed by silver paste on a copper substrate and mounted on the bottom of another chamber shown in Fig. 1.1. This chamber made of stainless steel (15 cm in diameter and 25 cm in height) was used for vacuum deposition of cerium metal, and there was a heater (tungsten coil) equipped 14 cm above the copper substrate on the bottom. Cerium metal (Santoku Kinzoku) was deposited on the nylon film in vacuo (less than 1.33×10^{-5} Pa) up to a content of 1.3 or 11.8 vol.%. Those contents corresponded to the thickness of 2 and 20 nm, respectively. During the vacuum deposition, the chamber had been cooled to 77 K by liquid nitrogen. Heat treatment of the composite films was done under the same vacuum condition for 10 min at 363 K, which was a temperature between the glass transition point and the melting point of nylon 11. Through the heat treatment, the cerium metal on the nylon 11 film was dispersed into the nylon layer in the form of ultrafine particles. The composite films were left in air after the heat treatment, so that the ultrafine particles produced were oxidized becoming cerium oxide.

1.2.2. HREM Observation of the Composite Films

High-resolution images were obtained with a Hitachi H-9000 transmission electron microscopy and operating at 300 kV ($C_s=0.9$ mm). Images were recorded under axial illumination at approximate Scherzer focus, with a point resolution better than 0.19 nm. The diameter of the

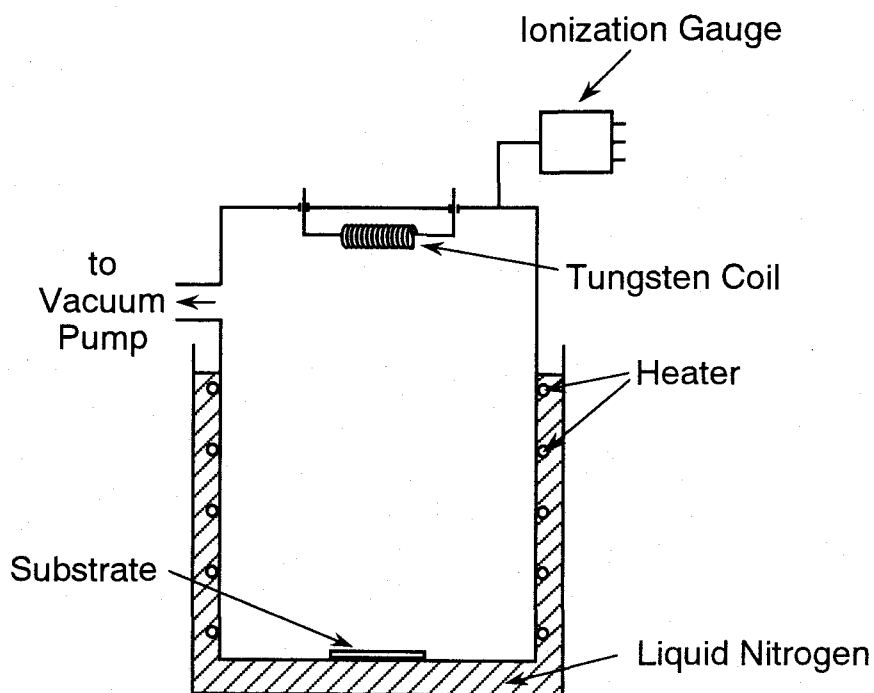


Figure 1.1. Apparatus for preparing CeO₂-nylon 11 composite films.

objective aperture used was 20 μm , which was large enough to include Debye-Sherrer rings from cerium oxide. The particle size distribution was determined by measuring the maximum diameter of more than 200 particles along a fixed direction on the HREM micrographs. Image simulation was also performed for a [111]-oriented model particle using the "MacHREMTM" program based on the multislice method.

1.2.3. UV-VIS Spectra Measurement

UV-VIS absorption spectra of the composite films were obtained on Shimadzu UV-2000 spectrometer. The CeO₂-nylon 11 composite films were prepared on silica glass plates for ultraviolet-visible absorption spectra measurements. The content of cerium metal layer was the same as the sample for HREM observation. The spectra for cerium oxide particles were obtained using a nylon 11 film after heat treatment as the reference.

1.3. Results and Discussion

1.3.1. Observation of Ultrafine Particles with a High-resolution Transmission Electron Microscopy

Figure 1.2 shows typical high-resolution electron micrographs (HREM) of the CeO₂-nylon 11 composite heated at 363 K for 10 min which contains 1.3 (Fig. 1.2(a)) and 11.8 vol.% (Fig. 1.2(b)) cerium oxide. It was evident from these figures that fine cerium(IV) oxide particles were dispersed uniformly and isolated individually in the nylon 11 matrix. The distance of the particles in the sample containing 1.3 vol.% CeO₂ is relatively shorter than the sample containing 11.8 vol.% CeO₂. HREM also showed well-defined lattice images of fine crystallites for most particles.

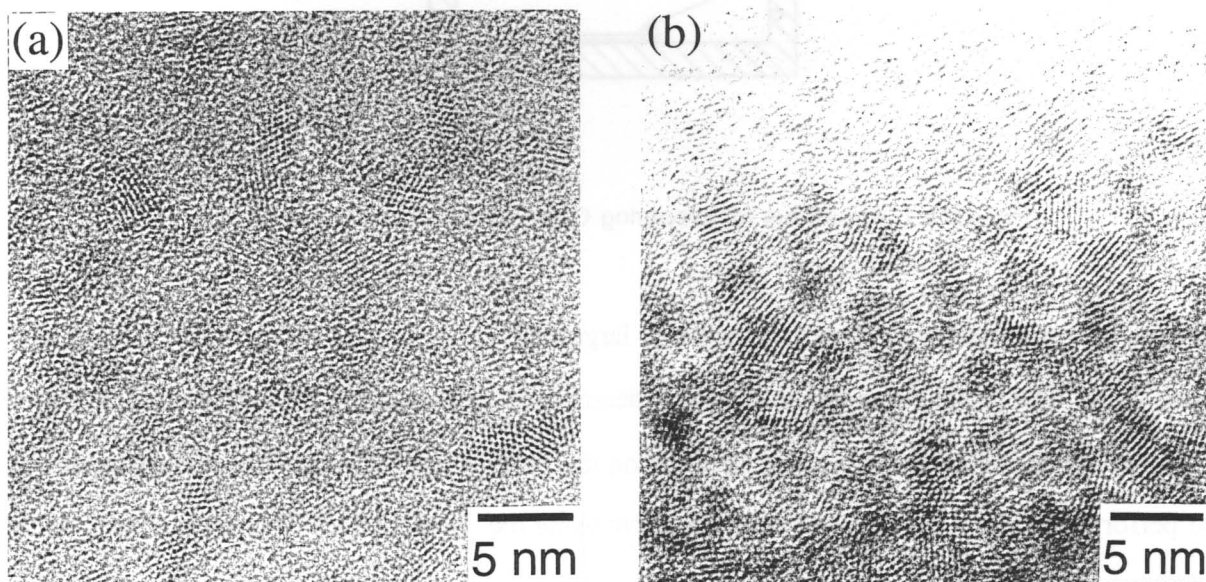


Figure 1.2. High-resolution electron micrographs of CeO₂-nylon 11 film with cerium oxide content of: (a) 1.3 vol.%, and (b) 11.8 vol. % after heating at 363 K for 10 min.

The particle size distribution was obtained by measuring the maximum diameter of each particle on the HREM micrograph. Figure 1.3(a) shows the particle size distribution of the sample contained 1.3 vol.% cerium oxide. It exhibited a relative narrow distribution. The particle sizes distributed between 1 and 8 nm, and the mean particle size was evaluated to be 4.1 nm. For the sample contained 11.8 vol.% cerium oxide particles, the sizes distributed between 2 and 22 nm as

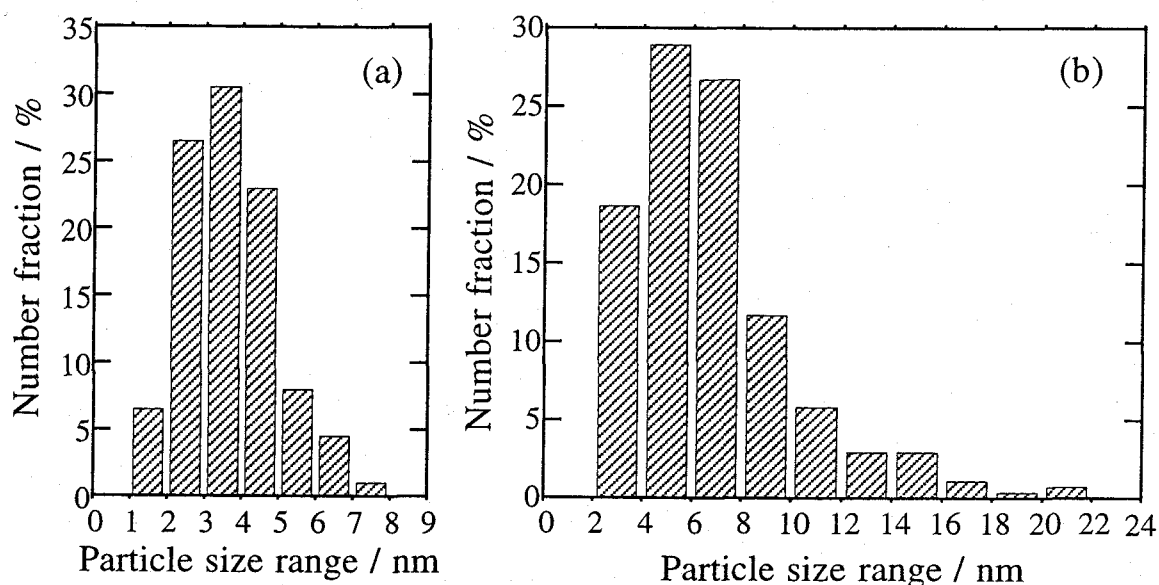


Figure 1.3. Particle size distribution of CeO₂ ultrafine particles in nylon 11 matrix measured from HREM micrographs: (a) 1.3 vol.% CeO₂, (b) 11.8 vol.% CeO₂.

shown in Fig. 1.3(b) and the mean particle size was 5.8 nm. Information on the lattice parameter and crystal structure of the particles was obtained from the selected-area electron diffraction patterns. Figure 1.4 shows an example of the diffraction patterns, and the Debye-Scherrer rings can be consistently indexed as those of cerium(IV) oxide with the cubic fluorite structure. The lattice constant calculated from the radius of each ring was 5.411 Å. This value was in good agreement with that given in the literature [31].

A typical HREM image of the CeO₂ particle is shown in Fig. 1.5(a), whereas a simulated image of [111]-oriented particle, with a crystal thickness of 20 slices of the planes and defocus of 500 Å, is illustrated in Fig. 1.5(b). The agreement between the two images was fairly good. All these facts indicate that the particles prepared by the RAD process are those of cerium(IV) oxide with the CaF₂ structure.

The mechanism of the RAD process taking place here to form the ultrafine particles is proposed as follows [29]. The polymer films prepared by means of vacuum deposition are in a thermodynamically metastable state. Heat treatment at the temperature between glass transition point and the melting point induces relaxation of the polymer and a drastic change of the film

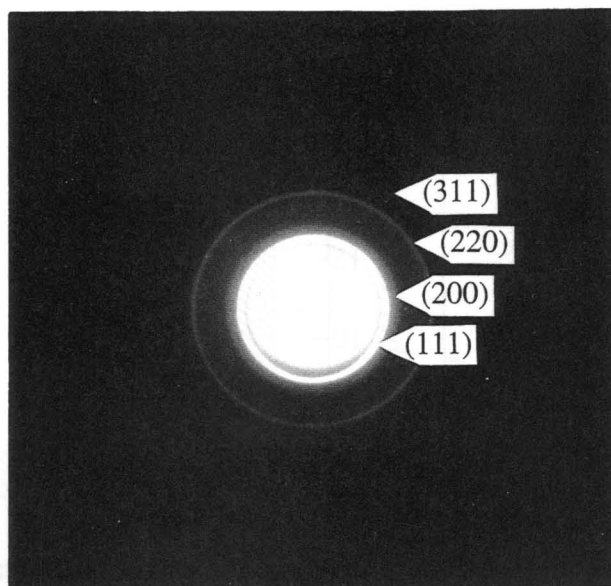


Figure 1.4. Electron diffraction pattern of CeO₂ ultrafine particles in nylon 11 matrix.

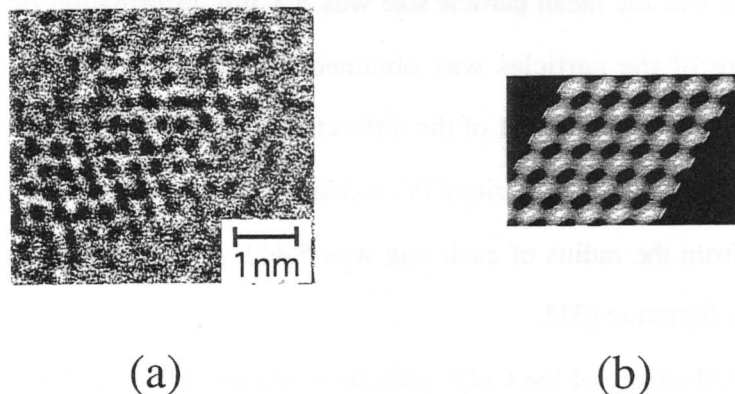


Figure 1.5. Experimental and simulation images of a CeO₂ particle in [111] orientation: (a) experimental image, (b) simulated image.

microstructure. During the heating and cooling process, the nylon 11 film returns to an equilibrium state with intermolecular rearrangement and changes into much stable structure. In this stage where the film is relaxed and stabilized through the heat treatment, the upper cerium metal film deposited on the surface of nylon 11 film is finely divided and is dispersed into the nylon matrix in the form of ultrafine metal particles.

However, rare earth metals are generally liable to be oxidized by air. Therefore, the cerium metal particles produced were partially changed to cerium oxide by oxidation with the residue of oxygen or water in the vacuum chamber. Moreover, when the samples were taken out of it after the heat treatment, they were completely oxidized by air.

The mean size of the particles in the composite film was dependent on metal contents; that is, the particle size became smaller when the content of cerium metal was decreased. One can explain the origin of this result as follows: During the heat treatment of a metal-polymer laminated film, the upper metal layer is destroyed and finely divided into the ultrafine particles with the relaxation of a lower polymer layer. The affinity of the stationary metal phase in the laminated film before the heat treatment will be proportional to the film thickness. Therefore, the thin metal layer on the polymer matrix was dispersed much more easily when compared with the thick one, and, as a result, the sizes of the ultrafine particles formed by the RAD process became smaller as the thickness of the metal layer decreased.

1.3.2. UV-VIS Spectra of CeO₂-nylon 11 Composite Films

As shown in HREM micrographs (see Fig. 1.2), the CeO₂ ultrafine particles obtained were uniformly dispersed in the nylon 11 matrix and their particle sizes were much smaller than the wavelength of ultraviolet and visible lights; the rays could transmit through the composite films easily. The absorption spectra of the CeO₂ ultrafine particles dispersed in nylon 11 film after the heat treatment, taking into account the absorption spectrum of a nylon 11 film of 150 nm thickness for blank, are shown in Fig. 1.6. The absorption edge evaluated from the spectrum for ultrafine particles was not clear. The particle size distribution is one of the possible reason, but probably not the dominant reason. From Fig. 1.6, the absorbance increases from as low as 650 nm, and this suggests that the band gap energy may be as low as 1.9 eV if particle size distribution is the dominant reason. This explanation for the absorbance tail at long wavelength in the absorption spectra of nanoparticle dispersion is most likely due to the light scattering by agglomerated particles or the absorption by surface state. Since the absorbance of the sample containing 11.8 vol.% CeO₂ (Fig. 1.6(b)) is always higher than that containing 1.3 vol.% CeO₂ (Fig. 1.6(a)), absorption by

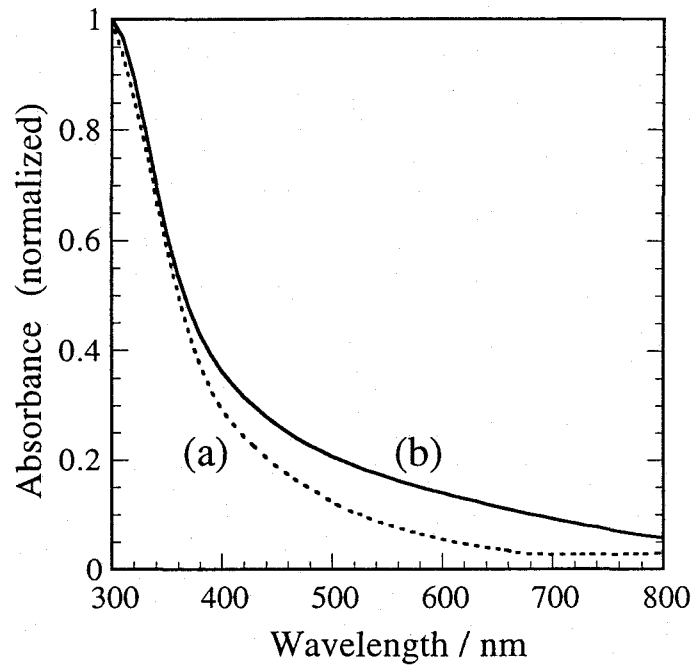


Figure 1.6. Absorbance spectra of CeO₂ ultrafine particles dispersed in nylon 11 films after heat treatment: containing (a) 1.3 vol.% CeO₂, (b) 11.8 vol.% CeO₂. The spectra were normalized at 300 nm.

surface state should not be the main reason. The only likely reason is then light scattering. This is also consistent with our common sense that the particle size and agglomeration in the sample loaded more CeO₂ should be much larger.

1.3.3. Optical Band Gap of CeO₂ Particles

The bandgap energy E_g for the CeO₂ particles is determined by extrapolation to the zero absorption coefficient which is calculated from the following equation [32]

$$\alpha = 2.303 \times 10^3 \frac{A\rho}{lC} \quad (1.1)$$

where A is the absorbance of a sample, $\log(I_0/I_t)$; ρ is the density of CeO₂ 7.28 g cm⁻³; C is the loading of the particles in g L⁻¹; and l is the path length. The optical absorption coefficient α near the absorption edge for indirect interband transitions is shown in the following equation [33]

$$\alpha \propto \frac{(h\nu + E_p - E_i)^2}{e^{(h\nu/kT)} - 1} + \frac{(h\nu - E_p - E_i)^2 e^{(h\nu/kT)}}{e^{(h\nu/kT)} - 1} \quad (1.2)$$

where E_i is the band gap energy for indirect transitions, $h\nu$ is the photon energy, and E_p is the phonon energy. For direct transitions, the optical absorption coefficient near the absorption edge is shown in the following equation [33]

$$\alpha \propto (h\nu - E_d)^{1/2} / h\nu \quad (1.3)$$

where E_d is the band gap energy for direct transitions.

A determination between the direct and indirect transitions can be made on the basis of the dependence of the absorption coefficient on the photon energy. Plots of $\alpha^{1/2}$ versus the photon energy from the spectral data of Fig. 1.6 displayed no linear relationships between 300 and 400 nm. By contrast, linear relationships were obtained when absorption coefficient data were plotted as $(\alpha h\nu)^2$ versus photon energy at wavelength shorter than 400 nm (Fig. 1.7). Therefore, the optical bandgap values of the samples for direct transition were calculated and discussed.

Figure 1.7 shows the plots of $(\alpha h\nu)^2$ versus the photon energy for the samples contained 1.3 and 11.8 vol.% cerium oxide particles in nylon 11 matrix, respectively. Here the intercept of the extrapolated linear portions gives the band gap for direct transitions. The calculated band gap values were 3.42 and 3.37 eV, respectively. These values are in fair agreement with the values between 3.34 and 3.38 eV, which were reported by Sundaram and Wahid [34] on CeO_2 films prepared by evaporation of Ce followed by oxidation through heating in O_2 . Similar results for the direct transition bandgap, with values between 3.5 and 3.6 eV were reported by Orel and Orel [35] for CeO_2 thin films prepared by sol-gel method. Therefore, it is concluded that there were no size quantization effects on the spectral properties of CeO_2 fine particles prepared in the present study. This may be due to the large mean size, relatively wide size distribution, and agglomeration of the particles.

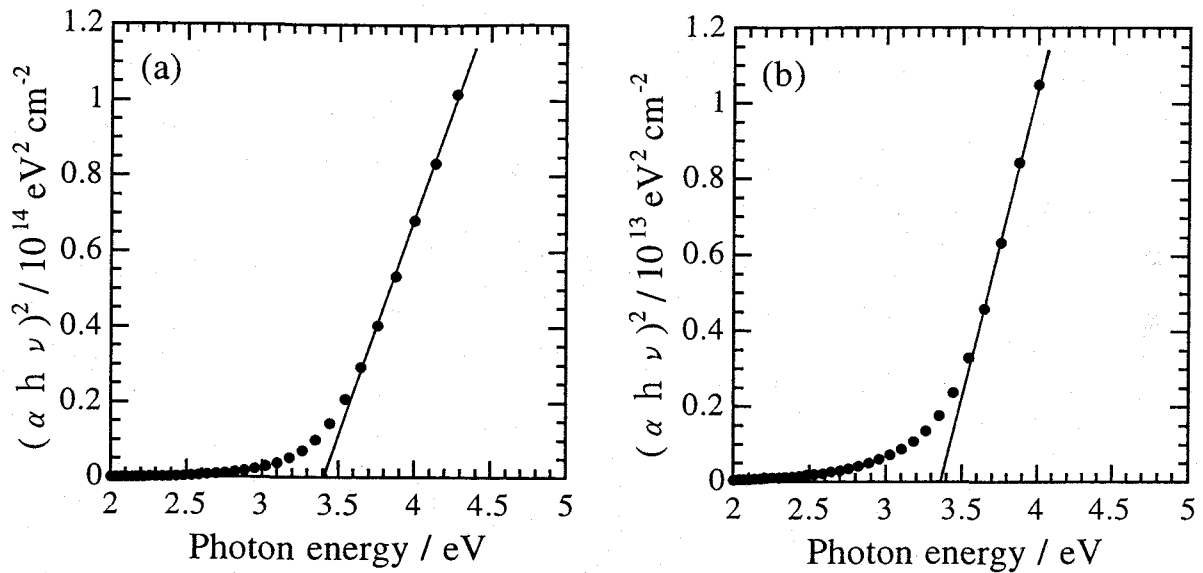


Figure 1.7. Plots of $(\alpha h \nu)^2$ versus photon energy for CeO₂ particles dispersed in nylon 11 films after heat treatment: (a) 1.3 vol.% CeO₂, (b) 11.8 vol.% CeO₂.

1.4. Conclusions

Nanometer-sized cerium(IV) oxide ultrafine particles prepared by the RAD process were uniformly dispersed and individually isolated in the matrix. Formation of the ultrafine particles by this process was due to the relaxation and stabilization of the polymer films in a thermodynamically metastable state. The mean particle size of cerium oxide decreased when its content was decreased because the affinity of the stationary metal phase in the laminated film before the heat treatment was proportional to the metal contents. The band gap energy of the CeO₂ fine particles were almost equal to those of the CeO₂ films previously reported.

Chapter 2

Characterization of Cerium(IV) Oxide Ultrafine Particles Prepared using Reversed Micelles

2.1. Introduction

From the results described in chapter 1, it became clear that the RAD process is useful to prepare nanosize cerium(IV) oxide fine particles. However, there were some problems in this method. Because the particles are present in a special condition like nylon 11 matrix, it is very difficult to separate the particles from the matrix as well as to make a lot of particles. Moreover, the mean particle size obtained from this process was not small as expected. Therefore, the another process was employed to make relatively a lot of particles with fine size.

The method described in this chapter is based on the use of microemulsions as reactors to obtain ultrafine and monodispersed nanoparticles. The microemulsion is generally defined as a thermodynamically stable system composed of two immiscible liquids and a surfactant. In water-in-oil microemulsions, the aqueous phase is dispersed as nanosize water droplets covered with a monolayer film of surfactant and co-surfactant molecules in a continuous nonpolar organic solvent such as hydrocarbon. Not only water but also aqueous solutions of metal salts or ammonia water can be soluble within the reversed micelles. These aqueous droplets encapsulated with surfactant molecules can continuously exchange their contents with one another when they collide. [22 - 25]. Therefore, if two kinds of water-in-oil microemulsions (one dissolves reactants A and another dissolves reactants B shown in Fig. 2.1) are mixed, a reaction between them takes place during the collisions of the water droplets in the microemulsions [26].

According to the above method, several studies have been carried out in recent years, and monodisperse ultrafine particles of metals [36 - 39] and oxides [40, 41] were synthesized in the dispersed phase of water-in-oil (W/O) microemulsion. Using this method enables us to obtain the

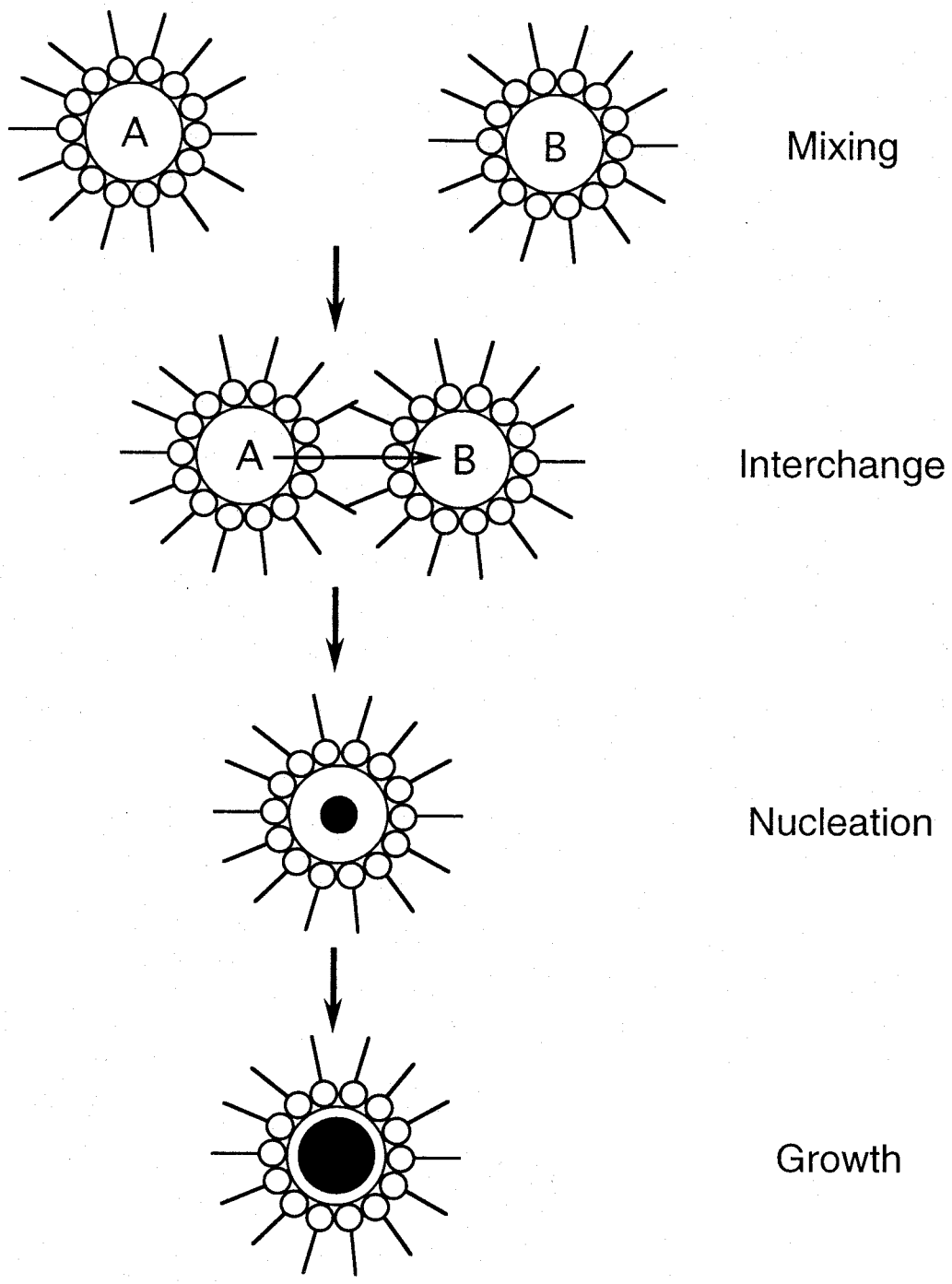


Figure 2.1. Schematic mechanism for the formation of particles in microemulsions [26].

particles with uniform small size and narrow size distribution, because the reaction field is limited inside of the fine reversed micelles. Nevertheless, rare earth compounds have not been synthesized by this method.

In this chapter, the microemulsion method was employed to prepare the smallest nanometer-sized cerium oxide ultrafine particles ever reported, and their size, morphology, and distribution were characterized with a high-resolution transmission electron microscopy (HREM). Also, the effect of fine size was estimated with the observation of ultraviolet-visible absorption property and catalytic behavior for CO oxidation of the particles.

2.2. Experimental Details

2.2.1. Chemicals

The materials used in this work were of the best quality commercially available. Polyoxyethylene (10) octylphenyl ether (OP-10, Wako Pure Chemical Industries Ltd.), cyclohexane (Kanto Chemical Co., Inc.), n-hexyl alcohol (Wako Pure Chemical Industries Ltd.), ammonium hydroxide (Nacalai Tesque, Inc.), acetone (Kanto Chemical Co., Inc.), and methyl alcohol (Wako Pure Chemical Industries Ltd.) were used without further purification. Also, the aqueous solution of cerium nitrate (Shin-Nippon Kinzoku Kagaku Co., Ltd.), aqueous solution of zirconyl nitrate (Shin-Nippon Kinzoku Kagaku Co., Ltd.), and γ -aluminum oxide (Shin-Nippon Kinzoku Kagaku Co., Ltd., Brunauer-Emmett-Teller (BET) specific surface area: $150 \text{ m}^2 \text{ g}^{-1}$) used were of high purity over 99.9%.

2.2.2. Synthesis

The preparation of the ultrafine cerium oxide particles was achieved by mixing two microemulsions containing cerium nitrate and ammonium hydroxide. The microemulsion system used in this work was composed of OP-10, cyclohexane, n-hexyl alcohol, and water solution. As OP-10 was only slightly soluble in cyclohexane solely, n-hexyl alcohol was added as a cosurfactant.

A microemulsion containing cerium salt was prepared as follows. First, OP-10 was mixed with n-hexyl alcohol in the molar ratio of 1:6.3 (weight ratio 1:1), and 12 - 180 mL of this solution was added to 200 mL cyclohexane with stirring until the mixture became transparent. Then, 2 mL of a cerium nitrate aqueous solution was added into the mixture and stirred until it became transparent again. The content of the cerium ion was varied so as to correspond to 0.093, 0.23, 0.46, and 0.93 mol L⁻¹. Another microemulsion solubilizing 15 mol L⁻¹ ammonium hydroxide was also prepared under the same procedure conditions described above. Then, the microemulsion containing cerium nitrate solution was mixed with another microemulsion containing ammonium hydroxide. The reaction mixture was stirred until a colloidal suspension formed. The particles were separated by centrifuging at a rate between 2.0×10^4 and 2.5×10^4 rpm for 1 h. After being successively washed with methyl alcohol, deionized water, and acetone by ultrasonic agitation, the fine powders were dried by freeze-drying and vacuum-drying.

The CeO₂/Al₂O₃ catalyst was prepared by almost the same procedure as that used for preparing the particles only. Twelve milliliters of OP-10 and n-hexyl alcohol mixture, 40 mL of cyclohexane, and 2 mL of a 0.93 mol L⁻¹ cerium nitrate aqueous solution were mixed with stirring until the mixture became transparent. Another microemulsion solubilizing 15 mol L⁻¹ ammonium hydroxide was also prepared with dispersed γ -aluminum oxide powders. Then, the microemulsion that contained the cerium nitrate solution was added into the solution containing ammonium hydroxide and γ -Al₂O₃ powders. In this process, the prepared CeO₂ ultrafine particles were supported on the surface of γ -Al₂O₃. The loading of the CeO₂ was 16.7 mol% (molar ratio of CeO₂/Al₂O₃ = 1/6). After the reaction mixture was stirred for 3 h, the suspension was centrifuged at 5×10^3 - 1×10^4 rpm for 1 h, and catalyst powder was obtained. The catalyst was washed successively with methyl alcohol, deionized water, and acetone. Finally, the powder was dried by the freeze-drying method followed by the vacuum-drying at 423 K for 1 h. The catalyst prepared in this method is denoted by ME catalyst hereafter. In addition, a coprecipitated catalyst was prepared to compare CO oxidation activities with that of a catalyst prepared by a microemulsion method. The coprecipitated catalyst was prepared by mixing of a cerium nitrate solution with ammonium hydroxide in which γ -aluminum oxide powders were dispersed, and

was washed and dried in a similar way to the ME catalyst. The catalyst prepared in a coprecipitated method is denoted by CP catalyst hereafter.

2.2.3. Instruments and Characterization

The ultrafine powders prepared by the microemulsion method were characterized by X-ray diffraction (XRD) using $\text{CuK}\alpha$ radiation (MAC Science M18XHF-SHA), High-resolution transmission electron microscopy (Hitachi H-9000), and differential thermal analysis (Rigaku TAS-100). The particle size and distribution were determined by measuring the maximum diameter of more than 200 particles on the HREM micrographs. Specific surface areas of the catalysts were measured by a conventional (BET) nitrogen adsorption method (Micromeritics Flow Sorb II 2300).

UV-vis absorption spectra of the cerium oxide particles dispersed in methyl alcohol were recorded using a Shimadzu UV-2000 spectrometer using a quartz cuvette (1 cm pathlength). Methyl alcohol was used as reference. The catalytic reactions for CO oxidation were carried out with 0.50 g of the catalyst in a conventional fixed-bed quartz tube reactor (10 mm o.d.) at 323 - 973 K. The inlet gas composition was 2% CO, 16% O₂ with He as balance, and the flow rate was adjusted to 25 mL min⁻¹. Products were analyzed by gas chromatography (Shimadzu GC-8A), and the CO oxidation activity of the ME catalyst was compared with that of the CP catalyst, both before and after the calcination at 1273 K in air for 5 h.

2.3. Results and Discussion

2.3.1. Characteristics of the CeO₂ Ultrafine Particles

The yield for the microemulsion process was between 60 and 70%, and it was confirmed from differential thermal analysis data that surfactant did not remain in the samples. During the process, we observed systematic changes in color of the precipitated particles in some cases. After the cerium nitrate microemulsion was mixed with the ammonium hydroxide microemulsion, the colorless transparent original solution immediately became translucent and gradually precipitated orange-colored fine particles. A colorless and clear supernatant was formed after the precipitation,

but the further color variance of the precipitate was observed. First, the color of the fine particles changed from orange to purple in about 30 min. Subsequently, the color of the precipitate gradually turned into pale purple, but the color variance was slower than the first change. Moreover, the color slowly changed to light yellow, and it took about 3 h to change completely. The wet centrifuged precipitate also appeared light yellow, but finally the freeze-dried powders were light brown.

These changes in color were observed in the cases that the particles were synthesized in low surfactant concentration. On the contrary, there was no color variance of the precipitate in high surfactant concentration. That is, the originally colorless transparent solution immediately only became orange-colored translucent and precipitation did not occur. This is due to the fact that the particles prepared within reversed micelles are stable in the solution at high surfactant concentration [42]. The color of the wet centrifuged particles also appeared orange, but the final freeze-dried powders were light brown.

Figure 2.2 shows a high-resolution electron micrographs of the ultrafine cerium(IV) oxide particles prepared by the microemulsion method. The content of water pool in reversed micelles is defined as the ratio of water to surfactant concentration, that is, $R_w = [H_2O]/[OP-10]$. In any case, it was evident from this figure that the particle size was very small, and the particle size decreased upon decreasing from $R_w = 15$ to $R_w = 1.5$, although the particles somewhat agglomerated one another. HREM also showed well-defined crystallites and their lattice images for most particles. BET specific surface area of the powders were between 153 and 185 $m^2 g^{-1}$. Assuming that all particles were spheres, their sizes calculated from the BET specific surface area were between 4.4 and 5.4 nm. These values seemed to be slightly larger than the HREM data because the dried powders were composed of agglomerated ultrafine powders.

X-ray powder diffraction of the CeO_2 nanoparticles obtained in this study is shown in Fig. 2.3(a). The diffraction pattern consistent with the cubic phases, but the width of the peaks were broad because of their small particle size. Therefore, in this case electron diffraction is a more valuable technique for characterization, and information on the lattice parameter and crystal structure of the particles were obtained from the selected-area electron diffraction patterns. Figure

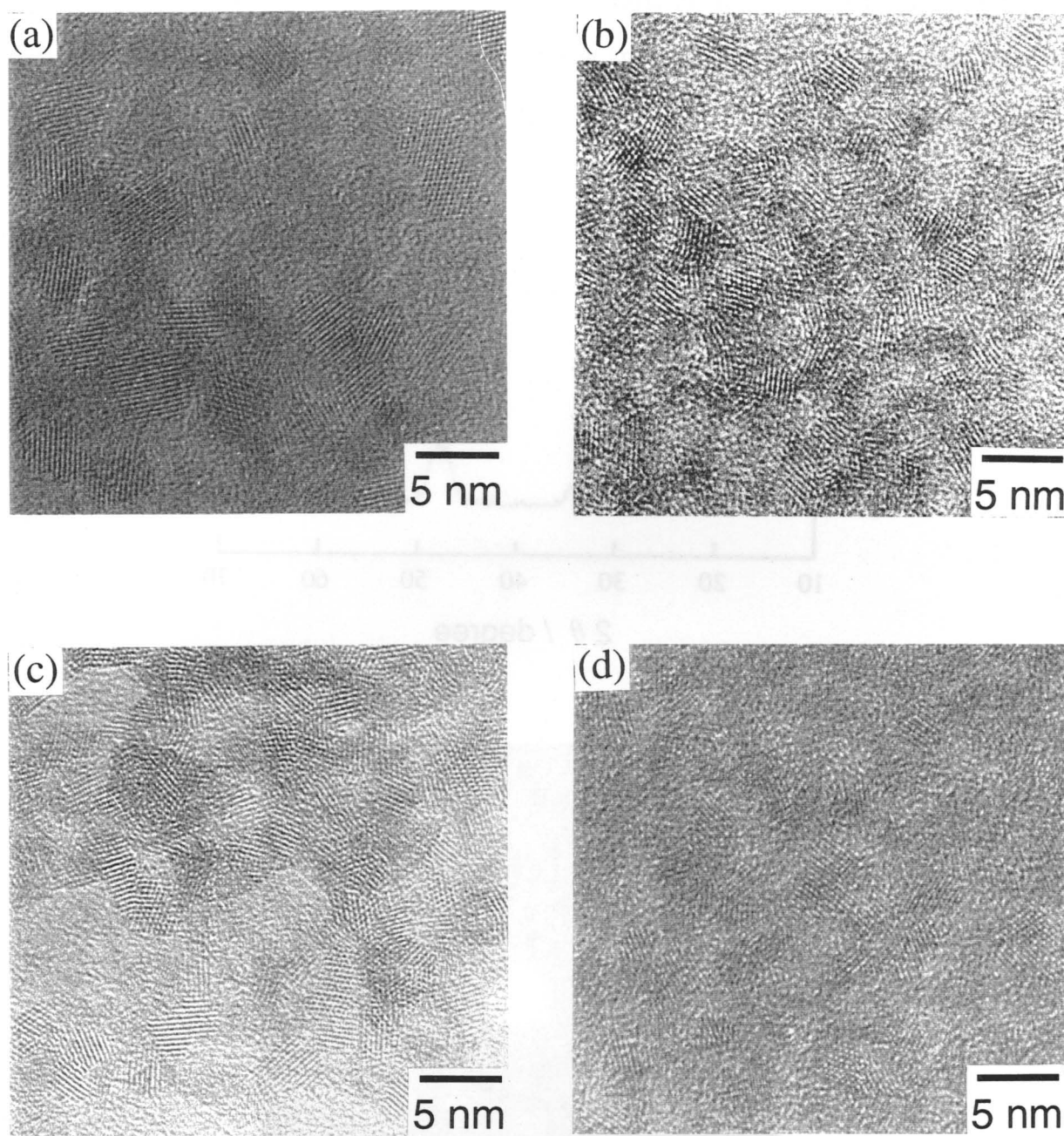


Figure 2.2. High-resolution electron micrograph of CeO₂ ultrafine particles by microemulsion method: These particles were prepared from 0.93 mol L⁻¹ cerium nitrate solution at (a) $R_w = 15$, (b) $R_w = 1.5$, or from 0.093 mol L⁻¹ cerium nitrate solution at (c) $R_w = 15$, (d) $R_w = 1.5$.

2.3(b) shows the diffraction patterns and the Debye-Scherrer rings of the particles. They can be consistently indexed as those of cerium(IV) oxide with the cubic fluorite structure, and the lattice constant calculated from the radii of rings was 0.541 nm. This value was in good agreement with that given in the literature [31].

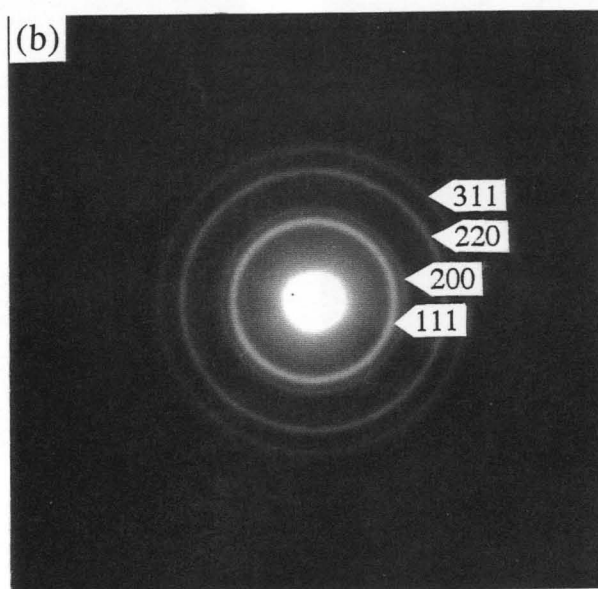
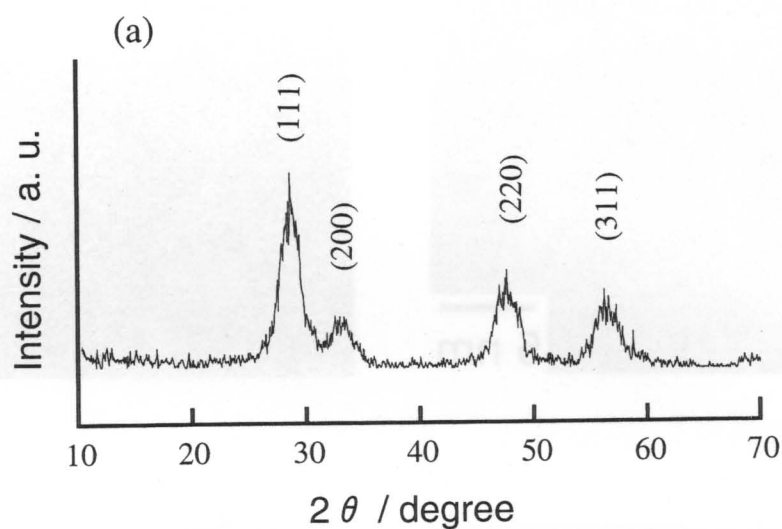


Figure 2.3. X-ray and electron diffraction pattern of CeO₂ ultrafine particles prepared by the microemulsion method.

These results presented in Fig. 2.3 showed that the precipitate from the reaction between cerium nitrate and ammonium hydroxide solutions in reversed micelles already exhibited the patterns of the CeO₂ crystallite. Chen et al. [4] previously reported that same behavior was observed by the direct reaction of cerium nitrate and ammonium hydroxide in the homogeneous precipitation method. In the literature, they concluded that this might be due to the addition of a large amount of NH₄OH because very high pH value was favorable for the oxidation of Ce³⁺ to Ce⁴⁺. The results in this study would be due to the same reason except there is a different point from their result. The difference is the color change of the particles. In the present results, the particle's color completely changed to light yellow before drying, while the homogeneous precipitated particles changed only after drying. The CeO₂ particles prepared by the microemulsion method were much smaller than the precipitated ones and were composed of 250 - 900 cerium ions, that is, 40 - 60 % of them was present at the surface. In the present sample, therefore, the surface energy was much higher and the oxidation of Ce³⁺ to Ce⁴⁺ had to be more completely driven than was the precipitated one.

2.3.2. Size Distribution and Mean Size of CeO₂ Particles

In the microemulsion method, the final size of the cerium oxide particles is restricted because the chemical reaction of cerium salt solution with ammonia water takes place inside the water droplets within the reversed micelles. Once the particles became a critical size in the water droplets, the surfactant molecules adsorbed on the surface of the particles to protect them against the further particle growth.

Figure 2.4 shows size distribution histograms of the cerium oxide particles prepared by using reversed micelles with different R_w values. At high water content, $R_w = 15$, the size distribution and mean particle size of the cerium oxide particles were relatively large. In contrast, at low water content, $R_w = 0.5$, the size distribution was very narrow and mean size was very small. The particle size change with the R_w value is shown in Fig. 2.5. The mean particle size was decreased from 4.1 to 2.7 nm when 0.93 mol L⁻¹ Ce(NO₃)₃ was used as starting material. In the case of 0.093 mol L⁻¹ Ce(NO₃)₃, the mean particle size was decreased from 3.4 to 2.6 nm. Here

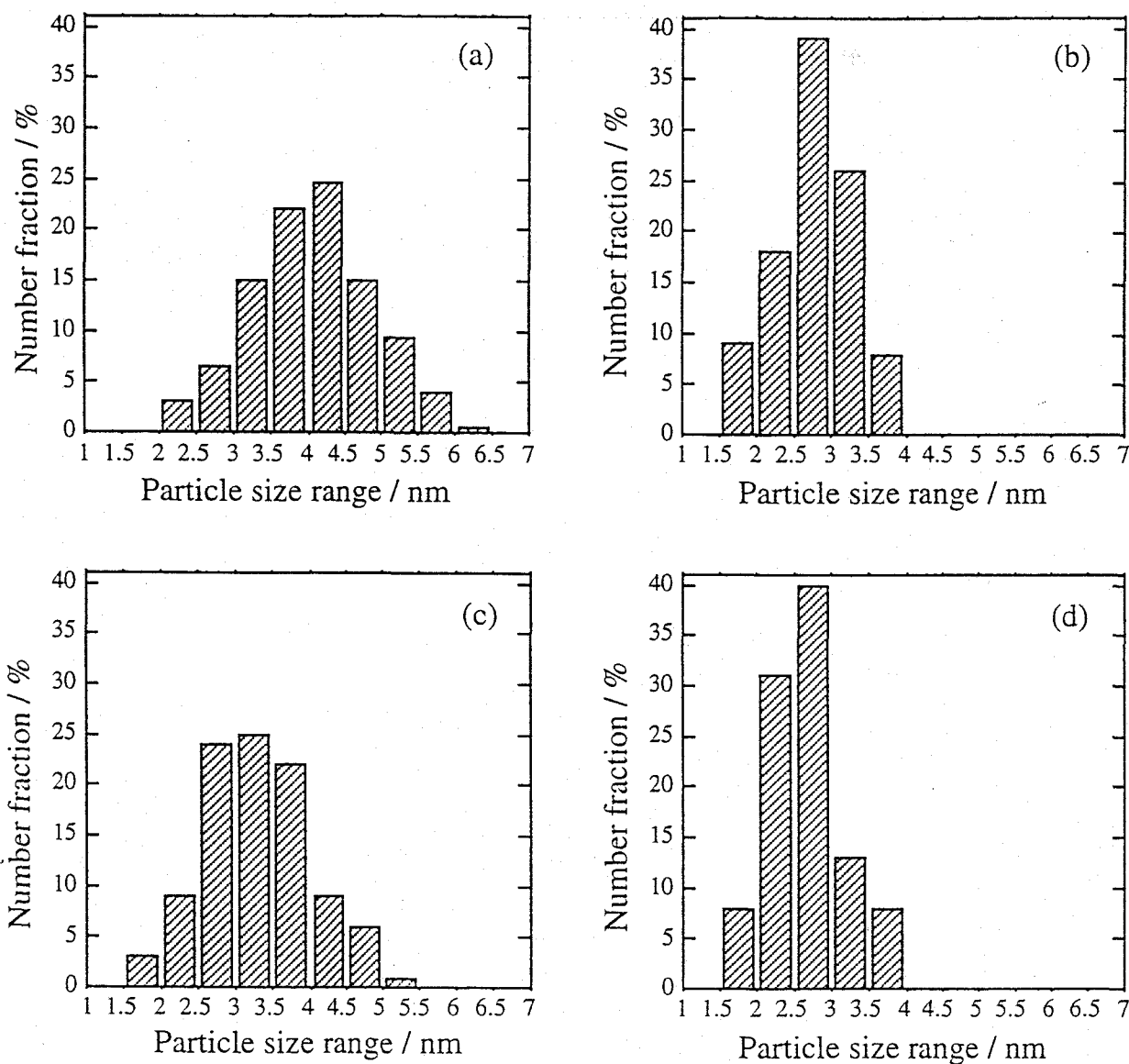


Figure 2.4. Particle size distribution histograms of CeO₂ ultrafine particles prepared from 0.93 mol L⁻¹ cerium nitrate solution at (a) $R_w = 15$, (b) $R_w = 0.5$, or from 0.093 mol L⁻¹ cerium nitrate solution at (c) $R_w = 15$, (d) $R_w = 0.5$.

the mean size, 2.6 nm was the smallest among the previous values reported for CeO₂ particles prepared by other methods.

The water droplet within reversed micelles is classified into two types of water [43]. One is the water which strongly interacts with the surfactant or cosurfactant molecules, and another is the water which behaves as bulk water. At low R_w , most of water is the former, and at high R_w , both of the former and the latter are present. In addition, it is known that the size of both reversed

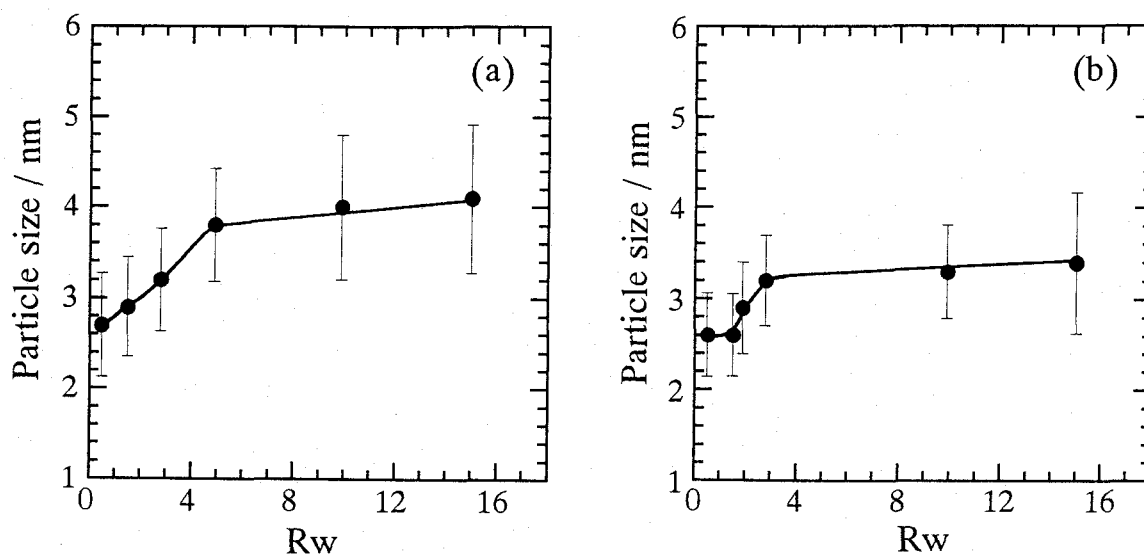


Figure 2.5. Mean particle size change of CeO₂ ultrafine particles prepared from (a) 0.93 mol L⁻¹ and (b) 0.093 mol L⁻¹ cerium nitrate solution at various Rw values.

micelles and water droplets increase with Rw value. As a result, the final size of the nanometer-scale particles can be varied by changing the amount of water solution solubilized in the system.

In the cases of Cu or Ag nanoparticles preparation using Aerosol OT as a surfactant, the change in the particle size with water content was elucidated by Pileni and co-workers [37 - 39]. They have explained the reason in terms of the facial water structure: At low water content, metal ions within reversed micelles strongly associate with surfactant or cosurfactant molecules, and they are not totally reacted. Our results support this explanation because the mean particle size did not decrease below 2.6 nm for the samples prepared from 0.093 mol L⁻¹ cerium nitrate solution (see Fig. 2.5(b)). This suggests that the size of 2.6 nm is the lower limit in the present system. On the other hand, the increase in the water content induces the extra free metal ions which react with reactant. This is responsible for the increase of the mean particle size. Electrostatic interaction between the surfactant and metal ions influence the reaction rate, but the balance in these remains constant upon increasing the water content. In addition, it is possible that more than one particle is formed in a reversed micelle at high Rw because the reaction space increases with water content. Therefore, at high water content above Rw = 9, the particle size was almost constant.

As mentioned above, it is known that the sizes of both the reversed micelle and the water

droplet depend on the R_w value. Therefore, if the concentration ratio of water to surfactant in W/O microemulsions is constant, the size of the particles seems to depend on the concentration of cerium ion. The distribution histograms of the cerium oxide ultrafine particles prepared at $R_w = 15$ are shown in Fig. 2.6. The concentration of cerium nitrate solution was changed so as to correspond to 0.093, 0.23, 0.46, and 0.93 mol L⁻¹. In all cases, the particles distributed in a range of 1.5 - 6.0 nm, and the particle distribution width was almost independent of the cerium nitrate concentration.

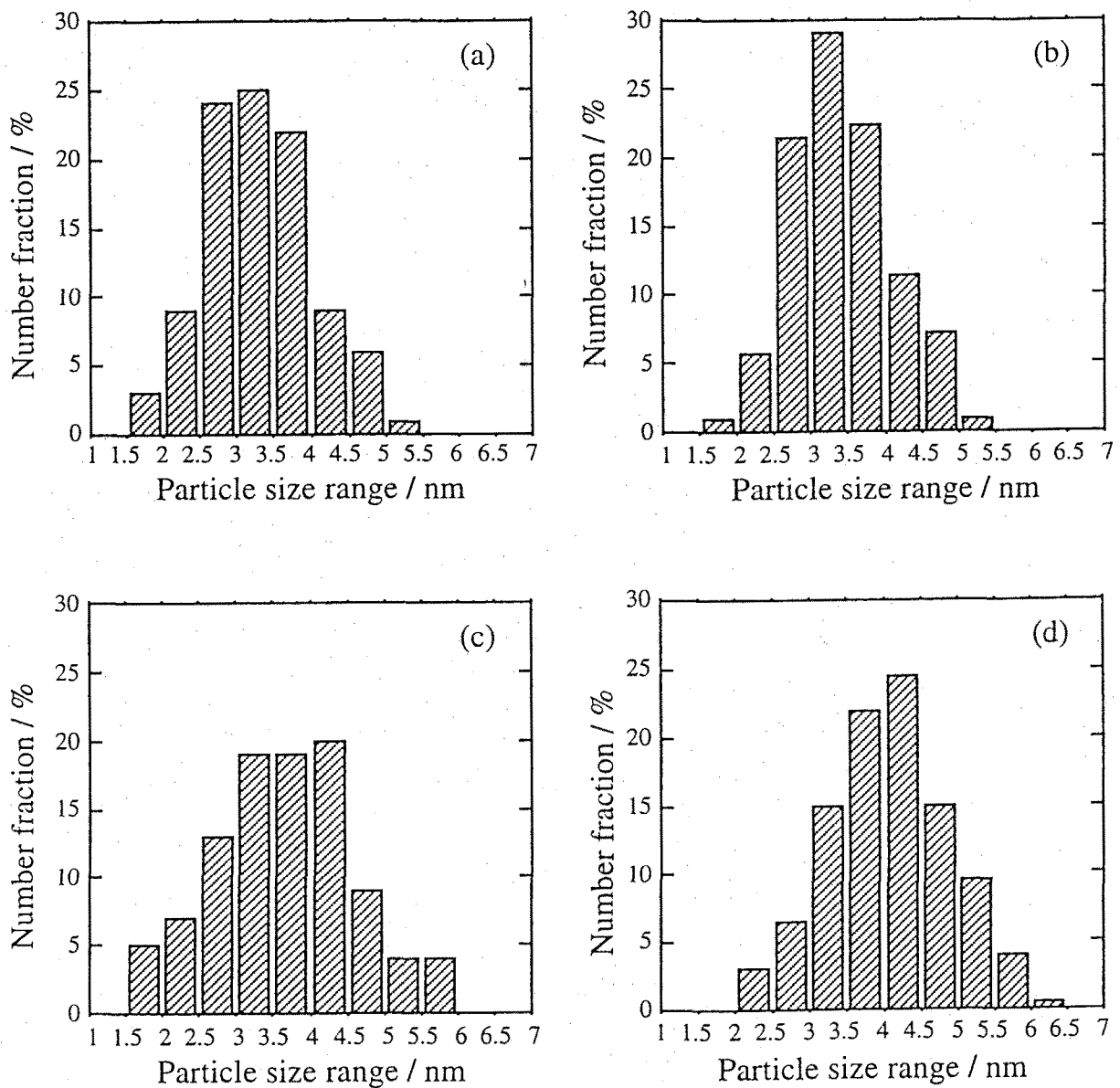


Figure 2.6. Particle size distribution of CeO₂ ultrafine particles at $R_w = 15$ prepared from (a) 0.093, (b) 0.23, (c) 0.46, and (d) 0.93 mol L⁻¹ cerium nitrate solution.

However, as the concentration of cerium nitrate increased, the peak of the distribution was slightly shifted to the larger particle size side. The particle sizes of the cerium oxide samples prepared from the solutions with various concentration of Ce^{3+} ion are summarized with standard deviations in Table 2.1. It is found that the higher the concentration of the cerium nitrate solution, the larger the mean CeO_2 particle size prepared. However, the largest mean size was not above 5 nm.

Table 2.1. Mean particle size of cerium(IV) oxide prepared at $Rw = 15$ for different concentrations of reactants

$[Ce(NO_3)_3]$ / mol L ⁻¹	Mean Particle Size / nm	Standard Deviation / nm
0.093	3.4	0.77
0.23	3.5	0.76
0.46	3.7	0.96
0.93	4.1	0.82

2.3.3. Absorption Spectra and Optical Band Gap of Ultrafine CeO_2 Particles

The ultrafine CeO_2 particles prepared in this study are materials that can prevent some damage from ultraviolet rays because they show strong absorption below 400 nm caused by charge transfer bands and block damage by UV radiation. Therefore, it is very important to characterize the optical properties of CeO_2 ultrafine particles for identification whether there is a specificity based on ultrafine size or not; however, there was no report on them.

Absorption spectra of the CeO_2 ultrafine particles dispersed in methyl alcohol, which were measured by taking into account the methyl alcohol for blank, are shown in Fig. 2.7. The spectrum for the specimen with the mean size of 2.6 nm is represented by a solid line and that of 4.1 nm corresponds to a dashed line. The concentration of the CeO_2 ultrafine particles was 4.6×10^{-4} mol L⁻¹ for both solutions, and these suspensions were transparent and colored with light yellow. Although the mean size of the particles decreased, the absorption edge obtained from the intersection of the tangent with the wavelength axis showed a weak blue shift.

The optical absorption coefficient α , the indirect (E_i) and direct bandgap energy (E_d) were calculated from the eqs. 1.1, 1.2 and 1.3 already described in detail in Chapter 1.

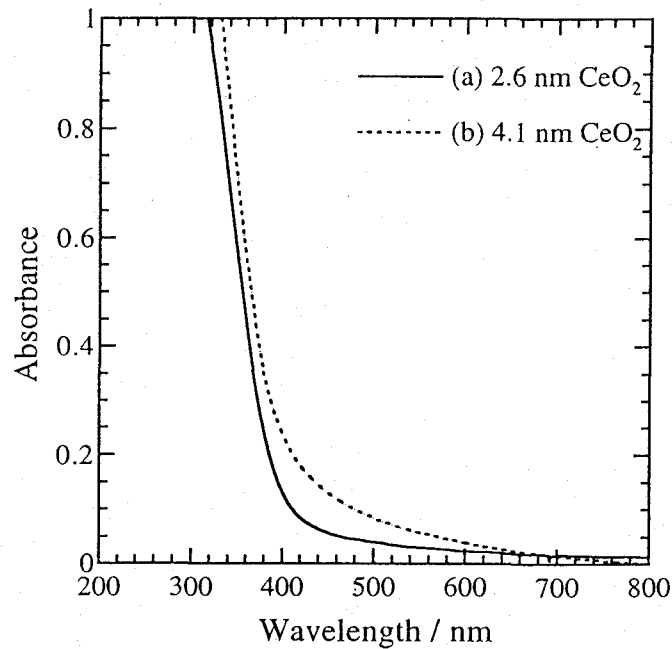


Figure 2.7. Absorbance spectra of CeO₂ ultrafine particles dispersed in methyl alcohol : The mean particle sizes are (a) 2.6 nm and (b) 4.1 nm, respectively.

Figure 2.8 shows the plots of $\alpha^{1/2}$ vs the photon energy for the CeO₂ particles with mean sizes of 2.6 and 4.1 nm. A linear extrapolation toward zero absorption gives E_i corresponding to indirect allowed transitions. The E_i values were 2.87 eV for the sample with 2.6 nm and 2.73 eV for that with 4.1 nm, respectively.

The plots of $(\alpha h\nu)^2$ versus the photon energy for the CeO₂ particles with the mean sizes of 2.6 and 4.1 nm are shown in Fig. 2.9. Also, the intersection of the extrapolated linear portions gives the band gap E_d for direct transitions, and the band gap values of them were 3.44 and 3.38 eV, respectively. Both of the indirect and direct bandgap energies increased with the decrease in the mean particle size, but the difference between them was small.

There are some reports on the band gap energy of CeO₂ thin film. Hogarth and Al-Dhhan [44] reported the E_i value to be 3.10 eV. Sundaram and Wahid [34] evaluated the bandgap energy for CeO₂ films prepared by evaporation of Ce followed by oxidation through heating in O₂ to be between 3.02 and 3.20 eV and between 3.34 and 3.38 eV, energy for indirect and direct transitions, respectively. Similar results between 3.0 and 3.12 eV for indirect transition and

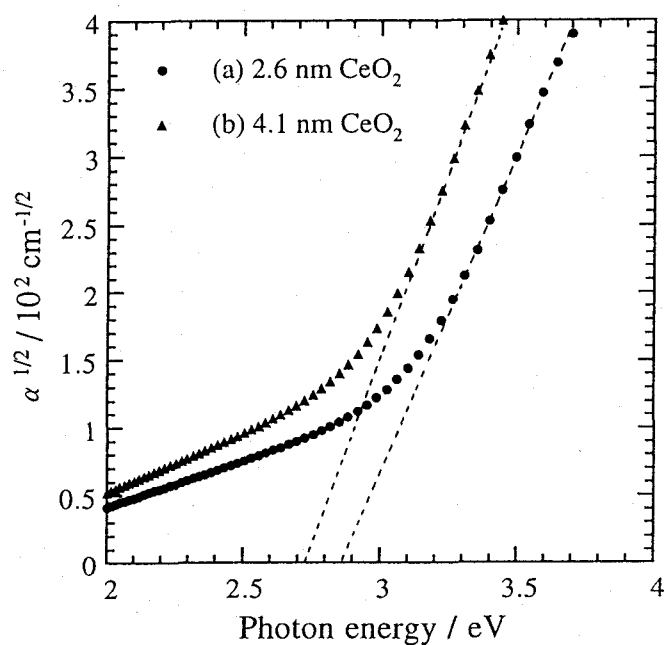


Figure 2.8. Plots of $\alpha^{1/2}$ vs photon energy for the CeO₂ particles dispersed in methyl alcohol : The mean particle sizes are (a) 2.6 nm and (b) 4.1 nm, respectively.

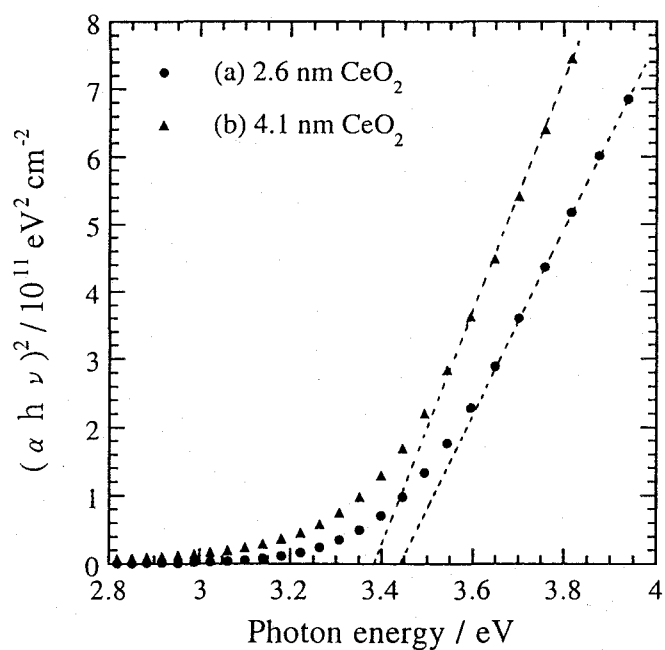


Figure 2.9. Plots of $(\alpha h\nu)^2$ vs photon energy for the CeO₂ particles dispersed in methyl alcohol: The mean particle sizes are (a) 2.6 nm and (b) 4.1 nm, respectively.

between 3.5 and 3.6 eV for direct transition were reported by Orel and Orel [35] for CeO₂ thin films prepared by a sol-gel method. These values are close to those of this study.

Moreover, the present values were almost equal to those of the ultrafine CeO₂ particles prepared by the RAD process, which were reported in Chapter 1. The mean particle size obtained by the RAD process were 4.1 and 5.8 nm, and they were larger than those prepared in this study. Nevertheless, their direct bandgap values calculated from eq. 2.2 were 3.42 and 3.37 eV, respectively, and they were in fair agreement with those of the samples prepared in the present study.

From these results, a little increase of bandgap energy with decreasing particle size was not due to the quantum size effect because the band gap energies obtained here were comparable to those of CeO₂ thin films and the CeO₂-containing composite films which were composed of nanosize CeO₂ crystalline particles. Therefore, it is concluded that there is no quantum size effect on the ultrafine CeO₂ particles at least over 2.6 nm.

2.3.4. Catalytic Activities of Ultrafine CeO₂ Particles Supported on Al₂O₃

As well as the ultraviolet absorbing property, it is known that cerium oxide shows high oxidation ability and oxygen storage capacity (OSC) [46], and the appearance of these functions are attributed to following two reasons. One is a low redox potential between Ce³⁺ and Ce⁴⁺, and the other is its structure [47]. The stable structure of cerium oxide at atmospheric pressure and room temperature is the cubic fluorite structure in which oxygen ions do not have a close-packed structure. Owing to this structure, cerium oxide can easily form many oxygen vacancies while maintaining the basic crystal structure. Although nanoparticles of cerium oxide have a great potentiality to be a high active catalyst because half of the cerium ions in the particles were present at their surface, there were a few reports on some catalytic properties based on their fine size [2, 48]. Then the size effect to the improvement in catalytic properties was discussed by using nanosize CeO₂ catalysts.

Powder XRD patterns for the as-prepared ME and CP CeO₂/Al₂O₃ catalysts showed diffraction peaks assigned to CeO₂ and γ -Al₂O₃. The width of these peaks were broad because of

their small crystalline sizes, but there were no differences between them. Although the crystallinity of both samples was improved to provide sharp diffraction peaks after the heat treatment in air at 1273 K for 5 h, there also were no clear differences between the ME and CP CeO₂ catalysts.

The catalytic activity tests for the ME and CP CeO₂/Al₂O₃ catalysts have been carried out to study the effect of small particle size and their preparation process on the oxidation of CO. Carbon dioxide was the only product for all catalysts. The activities of the ME and CP catalysts were compared in terms of their light off temperature corresponding to 50% conversion both before and after the heat treatment. The results are shown in Fig. 2.10, and the overall activity data and BET specific surface areas are summarized in Table 2.2. Before the heat treatment, CO oxidation activity of ME catalyst was higher than that of CP one. After the heat treatment in air at 1273 K for 5 h, the activities of the ME and CP catalysts were decreased. This would be due to the sintering of the fine particles impregnated on Al₂O₃, since the surface areas of them considerably decreased by the heat

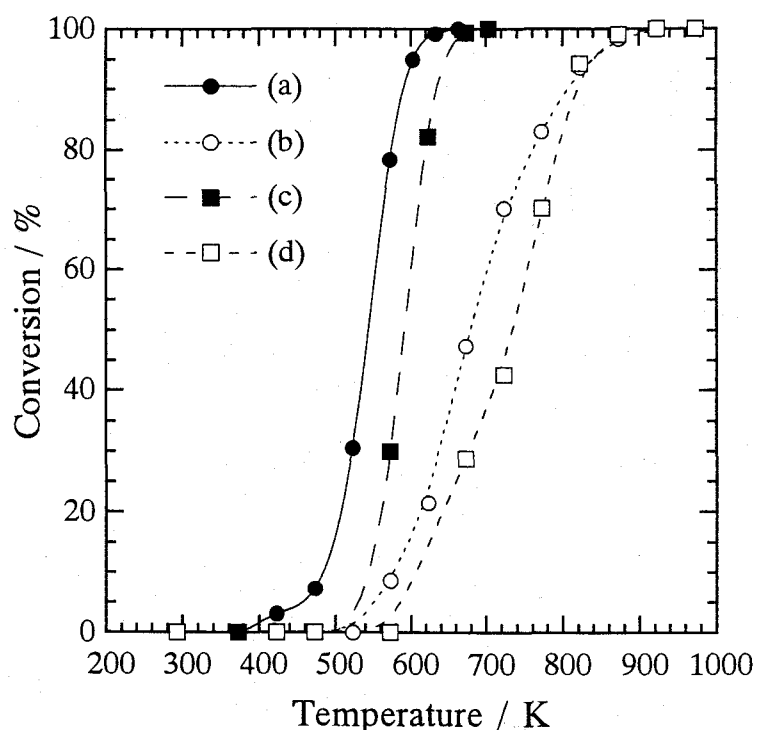


Figure 2.10. Catalytic activities for CO oxidation of (a) as-prepared ME CeO₂/Al₂O₃, (b) ME CeO₂/Al₂O₃ after being calcined at 1273 K for 5 h, (c) as-prepared CP CeO₂/Al₂O₃, and (d) CP CeO₂/Al₂O₃ after being calcined at 1273 K for 5 h. ME and CP represent that the catalysts were prepared by a microemulsion method and by a co-precipitation method, respectively.

Table 2.2. BET surface areas and activity data for the investigated catalysts ^a

Sample	Preheat temp. / K	B.E.T. surface area / m ² g ⁻¹	T / K (50%) ^b
CeO ₂ /Al ₂ O ₃ prepared by microemulsion method	423	165	543
	1273	73	680
CeO ₂ /Al ₂ O ₃ prepared by co-precipitation method	423	167	593
	1273	73	735

^a Amount of catalyst = 0.5 g, reaction gas mixture He : CO : O₂ = 82 : 2 : 16, flow rate = 25 ml min⁻¹.

^b Temperature for 50% conversion of CO to CO₂.

treatment (see Table 2.2). However, the ME catalyst still showed a higher activity, and the reaction temperature over this catalyst was lower by about 55 K for 50% conversion than over the CP catalysts. From these results, it is noted that the CeO₂/Al₂O₃ catalyst prepared by the microemulsion method shows higher activity despite the fact that its surface area is as same as that prepared by the coprecipitation method.

Haneda et al. [47] reported that the CeO₂/Al₂O₃ catalysts prepared by a sol-gel method using a needle boehmite sol derived from aluminum triisopropoxide, showed higher oxygen storage capacity after the H₂ reduction at 1173 K than those prepared by simple impregnation on an active alumina. They attributed the reason for high OSC to the high-dispersion state of CeO₂ particles and many oxygen vacancies, owing to the creation of new CeO₂ crystallite and CeO_{2-x} phases. Although the cause and the detailed mechanism of the high activities of ME catalyst have not been clear yet, they might be due to some effects such as fine size, morphology, and high OSC of the CeO₂ particles like the catalyst prepared by sol-gel method.

2.4. Conclusions

Nanometer-sized cerium(IV) oxide ultrafine particles were prepared by the microemulsion method and their size distribution was fairly narrow. The size of the CeO₂ particles was controlled easily in the vital range under 5 nm only by changing the concentration of the starting materials. The smallest mean size of the cerium oxide, 2.6 nm, prepared in this study was smaller than any

other values previously reported for CeO₂ particles.

The direct and indirect optical energy gaps of the particles obtained by the ultraviolet-visible spectrum measurement depended little on their mean size. Therefore, it is concluded that there are no size quantization effects on the spectral properties of CeO₂ fine particles prepared in the present study.

The CeO₂/Al₂O₃ catalyst prepared by the microemulsion method showed a much higher CO oxidation activity than that prepared by the coprecipitation method, both before and after the heat treatment at 1273 K for 5 h. Because the surface area values of them were almost equal, the reason for the high catalytic activity might be due to some effects such as fine size, morphology, and high OSC of the CeO₂ particles.

Chapter 3

Characterization and Catalytic Properties of Cerium-Zirconium Oxide Ultrafine Particles Prepared by the Microemulsion Method

3.1. Introduction

Recently, an environmental problem has been highlighted in a world scale. Among several causes to the destruction of the environment, effective cleaning of automobile exhaust gas is one of the important subjects and its improvement has been hoped for a long time. However, the existing three-way catalyst is not still enough to solve the problem and more improvement is necessary. Usually, the three-way catalyst converts three main pollutants such as CO, hydrocarbons, and NO_x contained in automobile exhaust gas simultaneously. But to establish high cleaning up efficiency, the air to fuel (A/F) ratio has to be controlled near the theoretical value (≈ 14.6) which is as-called the "window" [49]. The "window" is defined as the range of air to fuel ratios near the stoichiometric point over which conversion of each pollutant does not fall below a required value. Because the A/F ratio widely oscillate under the real car operation, it is monitored by the oxygen gas sensor and the ratio of air to fuel entering the converter is controlled systematically.

It is known that CeO₂ addition provides an improvement in the performance of the three way catalysts and the operational width of the "window" is decided by the oxygen storage capacity (OSC) of CeO₂ [46]. Since CeO₂ can easily absorb and desorb oxygen owing to its non-stoichiometric behavior [50], it can provide oxygen under rich fuel conditions and absorb it under lean fuel conditions. As a result, the width of the "window" enlarge. Moreover, the addition of it to the three way catalysts produces many important features such as thermal stabilization of alumina support [51], improving of the noble metal dispersion [52], and promotion of the water-gas shift reaction [53]. Therefore, CeO₂ is the most important component as a promoter in the three-way catalyst.

However, when the catalyst in the real automotive engine is undergone thermally severe conditions, deactivation took place by the sintering of CeO_2 . So, it has been recently studied to improve the performance of the promoter (CeO_2) in the three-way catalyst at high temperatures, and found that the reducibility and the thermal stability of CeO_2 is greatly enhanced by the mixing with zirconium oxide to form a $\text{CeO}_2\text{-ZrO}_2$ solid solution [54 - 60].

From the results reported in Chapter 2, it became clear that the microemulsion method was very useful to obtain ultrafine cerium oxide. In addition, no reference is reported on the preparation of the supported oxide catalysts using this method, although there are some references on the supported metal catalysts using microemulsions [36, 61, 62]. In this chapter, the microemulsion method was employed to synthesize the nanometer-sized $\text{CeO}_2\text{-ZrO}_2$ ultrafine particles, and this method was also applied to impregnate them on γ -aluminum oxide supports. Also, the CO oxidation activities of them were compared with those of conventional co-precipitated catalysts both before and after the calcination at 1273 K in air for 5 h to estimate their thermal stabilities.

3.2. Experimental details

3.2.1. Chemicals and Synthesis

The aqueous solution of zirconyl nitrate (Shin-Nippon Kinzoku Kagaku) with high purity over 99.9% was used other than the materials described in Chapter 2. The $\text{CeO}_2\text{-ZrO}_2$ particles and the $\text{CeO}_2\text{-ZrO}_2/\text{Al}_2\text{O}_3$ catalysts were also prepared by the microemulsion method. The microemulsion system used in this work was completely the same as described in Chapter 2. Instead of cerium nitrate solution, cerium and zirconyl nitrate mixed solution was used. The R_w value was fixed to 15 in this study. The concentration of cerium nitrate and zirconyl nitrate was fixed to 1.0 mol L^{-1} , and the mixing ratio of Ce:Zr was changed so as to correspond from 9:1 to 1:9. The coprecipitated $\text{CeO}_2\text{-ZrO}_2/\text{Al}_2\text{O}_3$ catalysts were also prepared to compare the activities.

3.2.3. Instruments and Characterization

The prepared particles and catalysts were characterized by BET specific surface area, XRD,

HREM, and CO oxidation activity. The apparatus and experimental conditions employed were the same described in Chapter 2. The CO oxidation activities of the catalysts prepared by the microemulsion method were compared with those of the catalysts prepared by the co-precipitation method. Hereafter, the catalysts prepared by the microemulsion method and those by the coprecipitated method are denoted by ME and CP catalysts, respectively.

3.3. Results and Discussion

3.3.1. BET Specific Surface Area

Generally, ultrafine particles have very high specific surface area because of their small sizes. This is very desirable for catalysts because catalytic reactions take place at the surface. Figure 3.1 shows the BET specific surface area of the as-prepared powders at various mixing ratio of cerium to zirconium. The surface area of them increased with zirconium content until the Ce:Zr molar ratio became 1:4, and the maximum value of $285 \text{ m}^2 \text{ g}^{-1}$ was obtained at this composition. Assuming

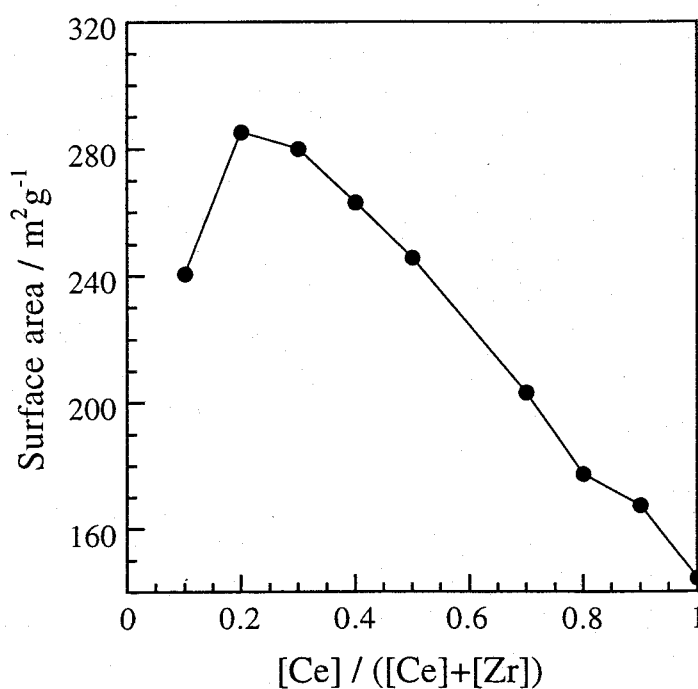


Figure 3.1. Composition dependence of the specific surface area of as-prepared $\text{Ce}_{1-x}\text{Zr}_x\text{O}_2$ ultrafine particles.

that all the particles were spheres, their sizes calculated from the BET specific surface area were between 3 and 5 nm. These values almost correspond to the mean size obtained from the HREM data (4 nm). Therefore, the increase of the specific surface area with zirconium content is mainly attributed to the increase of density of the particles. The sample containing 10 mol% cerium did not obey the linear relationship shown in Fig. 3.1. Being crystallized by calcination in air, the crystal system is monoclinic at this composition, while tetragonal phase is formed for cerium contents between 20 - 80 % [63 - 70]. Thus, there will be some differences such as density, particle growth and agglomeration state.

High specific surface area is one of the most important characteristics for catalytic reactions, and it is very important to keep high catalytic performance for the automotive exhaust catalysts. Therefore, the particles with the composition of Ce:Zr = 1:4 which had the highest specific surface area of $285 \text{ m}^2\text{g}^{-1}$, were characterized in detail hereafter.

3.3.2. XRD and HREM Observation

Figure 3.2 shows the X-ray powder diffraction patterns of the as-prepared and calcined nanoparticles (Ce:Zr = 2:8) obtained by the microemulsion method. The as-prepared powder (Fig. 3.2(a)) did not have definite patterns but showed halo one. Figure 3.3 shows the selected-area electron diffraction (SAED) pattern of the as-prepared particles, but obvious diffraction pattern could not be obtained, too. These results would be due to either that the particle size was very small or that the particles were amorphous. Therefore, in this case electron microscope observation are more valuable for characterization. Figure 3.4 shows a high-resolution electron micrograph (HREM) of the particles. It was evident from this figure that the particle size was very small and the particles were not agglomerated one another. The particles distributed between 2 and 11 nm, and the mean size was 4 nm. However, for most of the particles their lattice images were not shown in the HREM micrographs. These results clearly means that the as-prepared particles were amorphous.

In the real car operation, the automotive exhaust catalyst is used at wide temperature range from ambient one to 1273 K. In this case, the sintering of the particles at high temperature is a big

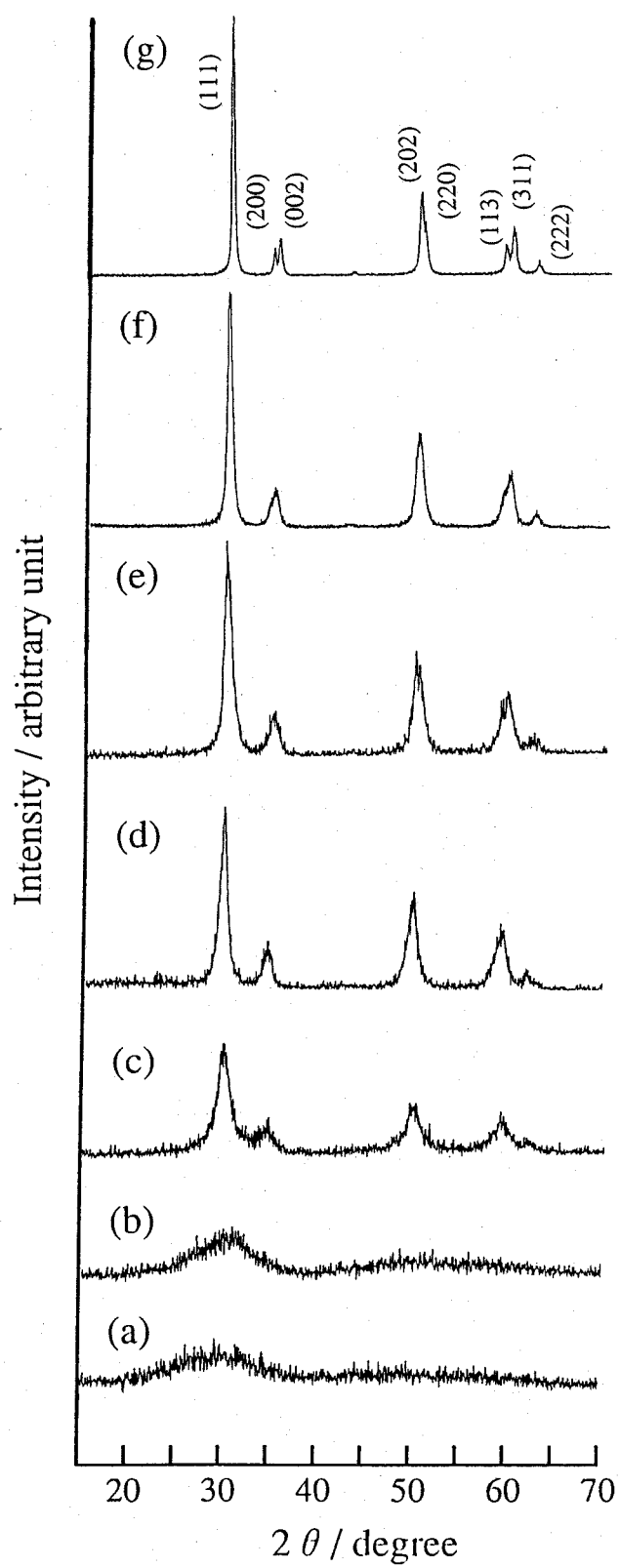


Figure 3.2. XRD patterns of CeO₂-ZrO₂ ultrafine particles (Ce:Zr = 2:8): (a); as-prepared, (b); calcined at 423 K, (c); 523 K, (d); 623 K, (e); 723 K, (f); 1023 K, and (g) 1273 K in air for 5 h.



Figure 3.3. Electron diffraction pattern of the as-prepared CeO₂-ZrO₂ ultrafine particles (Ce:Zr = 2:8).

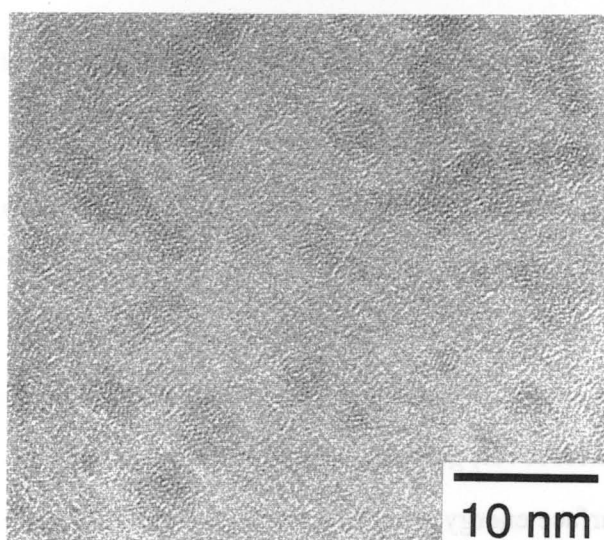


Figure 3.4. High-resolution electron micrograph of the as-prepared Ce_{0.2}Zr_{0.8}O₂ ultrafine particles.

problem for high catalytic performance, because it causes the decreasing of surface area. Then, the change in the specific surface area of the Ce_{0.2}Zr_{0.8}O₂ powder with calcination temperature was also examined (Fig. 3.5). The samples were calcined at various temperatures in air for 5 hours. The specific surface area was extremely decreased with increasing of the calcination temperature, and especially after the 1273 K treatment it was only 2 m²g⁻¹. The XRD patterns for the

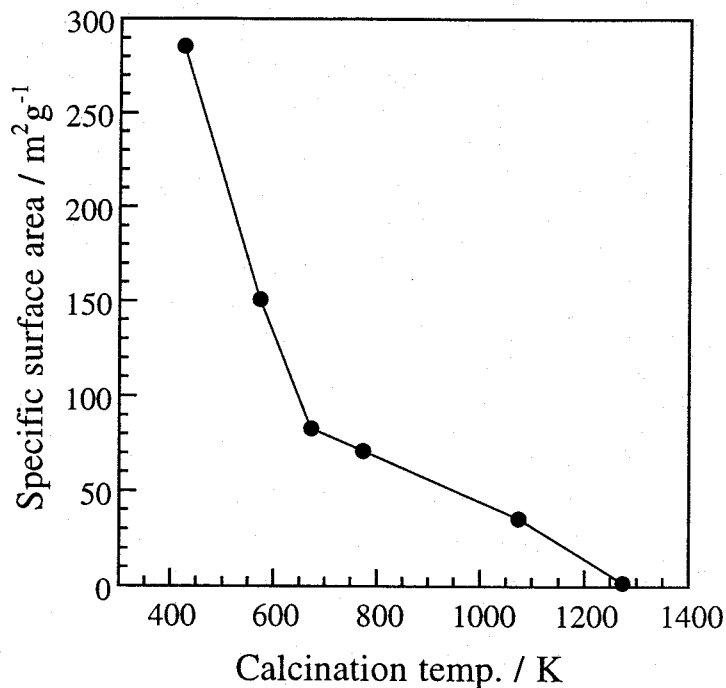


Figure 3.5. Specific surface area of $\text{Ce}_{0.2}\text{Zr}_{0.8}\text{O}_2$ ultrafine particles with various calcination temperatures.

$\text{Ce}_{0.2}\text{Zr}_{0.8}\text{O}_2$ particles calcined between 473 and 1273 K are also shown in Fig. 3.2. The crystallization of the particles was achieved between 473 and 673 K, and this result was corresponded to the abrupt decrease of the surface area shown in Fig. 3.5. Therefore, the decrease below and above 673 K would be mainly due to crystallization and sintering of the $\text{Ce}_{0.2}\text{Zr}_{0.8}\text{O}_2$ particles, respectively. Moreover, generally ultrafine particles are very easy to sinter one another because of their high surface energy, and, as a result, the particles had very small surface area after the calcination at 1273 K.

These above results clearly showed that the thermal resistivity of the ultrafine particles was very poor and that it was very difficult to keep high surface area after the calcination at high temperatures. Therefore, the particles were impregnated on gamma-alumina powders to improve their thermal resistivity of specific surface area. The surface area for as-prepared and calcined $\text{Ce}_{0.2}\text{Zr}_{0.8}\text{O}_2/\text{Al}_2\text{O}_3$ powders are summarized in Table 3.1. After the calcination in air at 1273 K for 5 h, the surface area of the particles which were not supported on alumina extremely decreased, but that of the impregnated ones kept relatively high surface area. Although these results suggest

Table 3.1. BET specific surface area of the $\text{Ce}_{0.2}\text{Zr}_{0.8}\text{O}_2$ and $\text{Ce}_{0.2}\text{Zr}_{0.8}\text{O}_2/\text{Al}_2\text{O}_3$ prepared by the microemulsion method

Sample	Preheat temp. / K	BET surface area / $\text{m}^2 \text{g}^{-1}$
$\text{Ce}_{0.2}\text{Zr}_{0.8}\text{O}_2$	423	285
	1273	2
$\text{Ce}_{0.2}\text{Zr}_{0.8}\text{O}_2/\text{Al}_2\text{O}_3$	423	183
	1273	82

that the thermal stability of the specific surface area of the fine particles were improved, it is not possible to estimate the thermal stability for catalytic activities only by means of surface area. Then, the activities were estimated both before and after the calcination at 1273 K by using CO oxidation which was known as one of common test reactions.

3.3.3. Catalytic Activity for CO Oxidation of Al_2O_3 -Supported Ultrafine CeO_2 - ZrO_2 Particles

The catalytic activity tests for $\text{Ce}_{0.2}\text{Zr}_{0.8}\text{O}_2/\text{Al}_2\text{O}_3$ catalysts prepared by the microemulsion method (ME) have been carried out to study the effects of small particle size and ZrO_2 addition on the reaction temperature in the oxidation of carbon monoxide. Carbon dioxide was the only product for all catalysts. The CO oxidation activities of the ME catalysts were compared with those of the ones prepared by the coprecipitation (CP) method in terms of their light off temperatures corresponding to 50% conversion both before and after the heat treatment at 1273 K. These results are shown in Fig. 3.6, and the overall activity data are summarized in Table 3.2 with their BET specific surface areas.

Before the heat treatment, CO oxidation activity of the ME $\text{Ce}_{0.2}\text{Zr}_{0.8}\text{O}_2/\text{Al}_2\text{O}_3$ catalyst was higher than that of the CP one, and the reaction temperature for 50% conversion over the ME catalyst was lower by about 140 K than over the CP one. It is very interesting to note that the microemulsion method is very effective to prepare the catalysts of high activities, and such activities mainly would be owing to fine size of the $\text{Ce}_{0.2}\text{Zr}_{0.8}\text{O}_2$ particles.

However, after the heat treatment in air at 1273 K for 5 h, the activities of both the ME and CP $\text{Ce}_{0.2}\text{Zr}_{0.8}\text{O}_2/\text{Al}_2\text{O}_3$ catalysts decreased. This would be due to the sintering of the particles

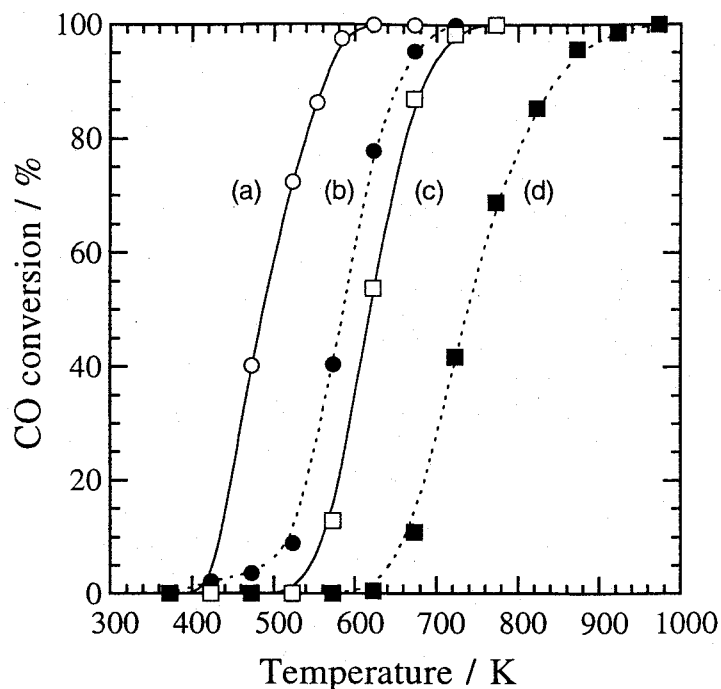


Figure 3.6. Catalytic activities for CO oxidation of (a) as-prepared ME $\text{Ce}_{0.2}\text{Zr}_{0.8}\text{O}_2/\text{Al}_2\text{O}_3$, (b) as-prepared CP $\text{Ce}_{0.2}\text{Zr}_{0.8}\text{O}_2/\text{Al}_2\text{O}_3$, (c) ME $\text{Ce}_{0.2}\text{Zr}_{0.8}\text{O}_2/\text{Al}_2\text{O}_3$ after being calcined at 1273 K for 5 h, and (d) CP $\text{Ce}_{0.2}\text{Zr}_{0.8}\text{O}_2/\text{Al}_2\text{O}_3$ after being calcined at 1273 K for 5 hours. ME and CP represent that the catalysts were prepared by a microemulsion method and by a co-precipitation method, respectively.

Table 3.2. BET surface areas and activity data for the catalysts prepared by the microemulsion method

Sample	Preheat temp./ K	B.E.T. surface area / $\text{m}^2 \text{g}^{-1}$	T/K (50%)
$\text{CeO}_2/\text{Al}_2\text{O}_3$ microemulsion method	423	165	545
	1273	73	680
$\text{Ce}_{0.8}\text{Zr}_{0.2}\text{O}_2/\text{Al}_2\text{O}_3$ microemulsion method	423	169	420
	1273	72	660
$\text{Ce}_{0.2}\text{Zr}_{0.8}\text{O}_2/\text{Al}_2\text{O}_3$ microemulsion method	423	183	483
	1273	82	593
$\text{Ce}_{0.2}\text{Zr}_{0.8}\text{O}_2/\text{Al}_2\text{O}_3$ co-precipitation method	423	183	620
	1273	75	740

deposited on Al_2O_3 surface, and no doubt the surface area of the catalysts decreased by the heat treatment. However, even after the calcination, the ME $\text{Ce}_{0.2}\text{Zr}_{0.8}\text{O}_2/\text{Al}_2\text{O}_3$ relatively kept high activity, and the reaction temperature over this catalyst was lower by about 150 K for 50%

conversion than over the CP one. Moreover, even after the heat treatment, the ME catalyst showed higher activity than that of the CP one with no heat treatment.

Powder XRD patterns for the as-prepared ME and CP $\text{Ce}_{0.2}\text{Zr}_{0.8}\text{O}_2/\text{Al}_2\text{O}_3$ catalysts showed halo patterns because the $\text{Ce}_{0.2}\text{Zr}_{0.8}\text{O}_2$ particles were amorphous. However, after the heat treatment in air at 1273 K for 5 h, the XRD patterns of both samples showed sharp diffraction peaks which was assigned to tetragonal ZrO_2 -based solid solution. Another diffraction peaks were not detected except for γ - Al_2O_3 .

The crystalline sizes of the calcined samples were determined from the X-ray line broadening using Scherrer's equation:

$$D = 0.9 \lambda / (\beta \cos \theta) \quad (3.1)$$

where D is the average diameter of crystallites, λ is the wavelength of the x-rays, θ is the diffraction angle, and β is the full width at half maximum of the peak. After the heat treatment, the average crystalline size of the $\text{Ce}_{0.2}\text{Zr}_{0.8}\text{O}_2$ particles in the ME and the CP catalysts were 17 and 19 nm, respectively. In addition, TEM images of them were also observed as shown in Fig. 3.7. Although the particles sintered and grew larger by the heat treatment, the particle size of

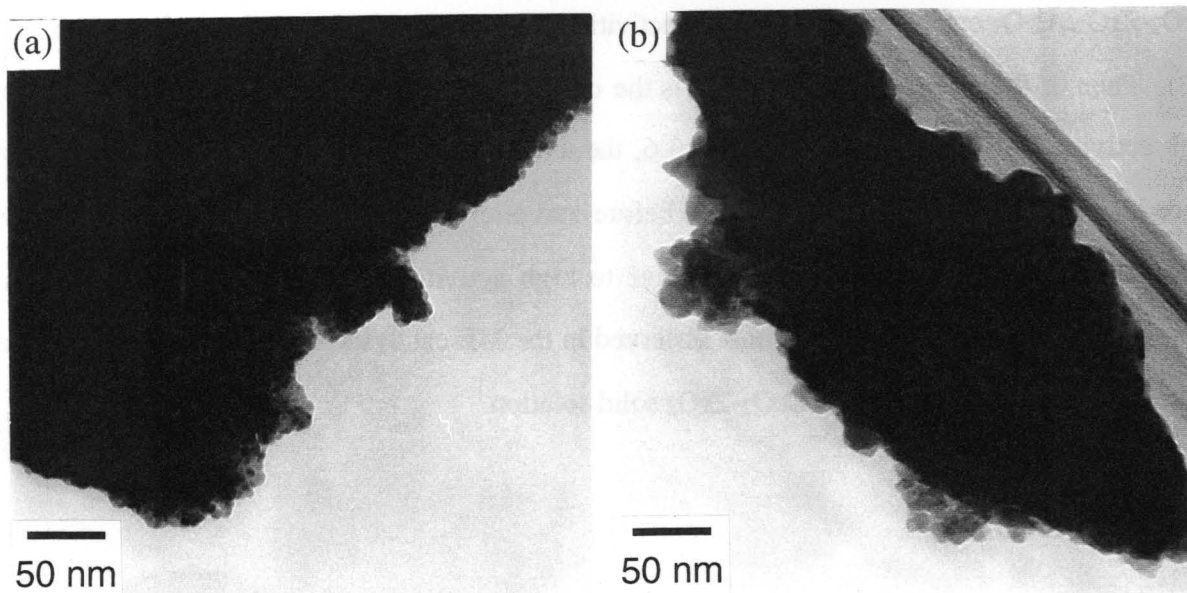


Figure 3.7. TEM photograph of (a) ME $\text{Ce}_{0.2}\text{Zr}_{0.8}\text{O}_2/\text{Al}_2\text{O}_3$ and (b) CP $\text{Ce}_{0.2}\text{Zr}_{0.8}\text{O}_2/\text{Al}_2\text{O}_3$ after being calcined at 1273 K for 5 h. ME and CP represent that the catalysts were prepared by a microemulsion method and by a co-precipitation method, respectively.

$\text{Ce}_{0.2}\text{Zr}_{0.8}\text{O}_2$ in the ME catalyst was obviously smaller than that in the CP one. These results clearly shows that the particles supported on alumina by the microemulsion method are more stable against sintering than those supported by the coprecipitation method.

The CO oxidation activity of the ME $\text{Ce}_{0.8}\text{Zr}_{0.2}\text{O}_2/\text{Al}_2\text{O}_3$ catalyst was also examined to identify the composition dependence on the catalytic activities. The overall activity data and their BET specific surface areas are also summarized in Table 3.2 with the results for $\text{CeO}_2/\text{Al}_2\text{O}_3$ already described at Section 2.3.4 in Chapter 2. Compared the results of $\text{CeO}_2\text{-ZrO}_2/\text{Al}_2\text{O}_3$ with those of $\text{CeO}_2/\text{Al}_2\text{O}_3$, the activities of the former were higher than that of the latter both before and after the calcination.

The redox properties of ceria and the high mobility of oxygen contribute to the catalytic reactivity in total oxidation reactions. It has been reported that the reduction temperatures from Ce^{4+} to Ce^{3+} decreased with increasing ZrO_2 content by TPR measurements of zirconium-doped CeO_2 under flowing H_2 gas [55]. Zirconium addition also prevents the grain growth of crystallites at high temperatures [51], and the reaction between CeO_2 and Al_2O_3 under reducing atmosphere [59]. These results shows that addition of ZrO_2 produces higher particle dispersion and greater range of reversibility of the $\text{Ce}^{4+}/\text{Ce}^{3+}$ redox reaction by forming $\text{CeO}_2\text{-ZrO}_2$ solid solutions. In fact, the $\text{CeO}_2\text{-ZrO}_2/\text{Al}_2\text{O}_3$ catalysts showed higher activities than those of $\text{CeO}_2/\text{Al}_2\text{O}_3$ catalysts (see Table 3.2). Then, if the effect of ZrO_2 loading is the only factor, the CP catalysts also ought to show high activity. However, as shown in Fig. 3.6, the activities of the CP $\text{Ce}_{0.2}\text{Zr}_{0.8}\text{O}_2/\text{Al}_2\text{O}_3$ catalyst were less than those of the ME one both before and after the heat treatment. These results also show that the preparation process contribute to high activities as well as ZrO_2 doping, and, therefore, the reason for high activities observed in the ME catalysts is attributable to both small crystalline size and formation of $\text{CeO}_2\text{-ZrO}_2$ solid solution.

3.4. Conclusions

Nanometer-sized ceria-zirconia ultrafine particles were prepared by the microemulsion method and the as-prepared particles were amorphous. The heat resistance of the particles prepared

was very small, and the specific surface area extremely decreased after calcination at 1273 K. However, the decrease of the surface area was inhibited by impregnating the particles on alumina support.

The $\text{Ce}_{0.2}\text{Zr}_{0.8}\text{O}_2/\text{Al}_2\text{O}_3$ catalyst prepared by the microemulsion method showed much higher CO oxidation activity than that of the same catalyst prepared by the coprecipitation method both before and after the heat treatment at 1273 K for 5 h. Since the particle size of the catalysts prepared by the microemulsion method remained small, the reason for the high catalytic activity was attributed to fine particle size.

The CO oxidation activities of the $\text{CeO}_2\text{-ZrO}_2/\text{Al}_2\text{O}_3$ catalysts prepared by the microemulsion method were higher than that of the $\text{CeO}_2/\text{Al}_2\text{O}_3$ catalyst, and this would be due to some effects such as formed phase and surface composition of the catalysts.

From all the results obtained in this study, it is obvious that the microemulsion method is superior to preparing the high heat resistant catalysts that can keep high activities even after undergoing in a severe heat condition.

Chapter 4

Reduction Behavior of Cerium-Zirconium Oxide Prepared by Means of a New Synthesis Method Using Thermal Decomposition of Cerium Zirconyl Oxalate

4.1. Introduction

As mentioned in Chapter 3, CeO_2 is an important component to the three-way catalysts because of its high oxygen storage capacity (OSC). For CeO_2 , high surface area is essential to obtain a significant OSC since the redox processes occur in the three-way catalysts essentially on the surface [46, 53]. For this reason, investigation on thermal stability of the CeO_2 component is of current interest and it has been reported that thermal stability of CeO_2 is improved by ZrO_2 addition [54 - 60].

Recently, Fornasiero and co-workers [56] investigated the redox properties of a number of Rh-loaded $\text{Ce}_x\text{Zr}_{1-x}\text{O}_2$ ($x=0.1-0.9$) solid solutions prepared by a high temperature solid state reaction and they observed a strong promotion of the reduction of the mixed oxide support due to the incorporation of ZrO_2 into the CeO_2 framework. Reductions of the support occurred in the bulk at the temperature between 600-700 K which allows one to obtain high OSC notwithstanding the very low surface areas (about $1 \text{ m}^2 \text{ g}^{-1}$) of the samples investigated. It was also clearly shown that the redox behavior of $\text{Ce}_x\text{Zr}_{1-x}\text{O}_2$ ($x=0.1-0.9$) strongly depends on both the composition and the structure of the solid solution: the cubic $\text{Ce}_{0.5}\text{Zr}_{0.5}\text{O}_2$ sample was the easiest one to be reduced.

Moreover, they also disclosed that a $\text{Ce}_{0.5}\text{Zr}_{0.5}\text{O}_2$ mixed oxide also showed an unusual improvement of the redox behavior upon sintering induced by a repetitive reduction/oxidation of the solid solution [57, 58]. They attributed this enhancement of the reducibility to an increased oxygen mobility in the bulk induced by the addition of the Zr into the CeO_2 lattice which gives unusual redox properties to these systems.

Similar results were also reported by Yao and co-workers [71]. They employed the CeO₂-ZrO₂ which was reduced at 1323 K in Ar+H₂+H₂O gas mixtures and reoxidized at 873 K in O₂ gas, and clarified that the obtained CeO₂-ZrO₂ showed an unusual improvement of the reduction behavior than the samples only calcined in air. The evolution behavior of oxygen from CeO₂-ZrO₂ powders at low temperatures was explained on the basis of the appearance of cubic pyrochlore type structure.

In this Chapter, CeO₂-ZrO₂ solid solutions are prepared by thermal decomposition of oxalate in argon flow and following oxidation in air. The reduction behavior of the obtained CeO₂-ZrO₂ powders are investigated and compared with the samples prepared by the other methods already reported to obtain CeO₂-ZrO₂ powders with high redox property. The aims are to prepare cubic Ce_{0.5}Zr_{0.5}O₂ with pyrochlore type structure by thermal decomposition of oxalate and to verify the influence of the preparation process of the solid solution on the reduction processes.

4.2. Experimental details

4.2.1. Chemicals and Synthesis

The materials used were the same as those described in Chapter 3 except γ -aluminum oxide, and oxalic acid (Wako Pure Chemical Industries Ltd.) with the best quality commercially available was used.

Cerium zirconyl oxalate powders were prepared by the coprecipitation as well as the microemulsion method. The concentration of cerium nitrate, zirconyl nitrate, and oxalic acid aqueous solution were fixed to 0.5 mol L⁻¹, and the mixing ratio of Ce:Zr was adjusted from 4:6 to 5:5.

In the coprecipitation method, 40 mL of the mixed solution of cerium nitrate and zirconyl nitrate was added to 55 mL of oxalic acid solution. To facilitate the precipitation, 3 mol L⁻¹ ammonium hydroxide was added until the pH value of the solution became about 2, and then, 80 mL of acetone was added. After keeping for overnight the white colored precipitate was filtered, washed with water and acetone in succession, and dried at 393 K in air.

The microemulsion system used in this work was similar as described in Chapters 2 and 3, and the R_w value was also fixed to 15. The microemulsion solubilizing cerium and zirconyl nitrate solution was mixed with the another one solubilizing oxalic acid solution. The reaction mixture was stirred until the solution was suspended by formed colloidal particles, and the microemulsion solubilized 3 mol L⁻¹ ammonium hydroxide were added until pH = 2. Then, 30 mL of acetone was also added to get high yields. The particles were separated by centrifuging, and washed with methyl alcohol, deionized water and acetone successively. The obtained fine powders were dried at 393 K in air.

The cerium zirconium oxalate powders were decomposed at 1273 K in Ar flow for 5 h, and obtained CeO₂-ZrO₂ powders were calcined at 673 K in air for 2 h. Hereafter, the samples prepared from oxalate by the coprecipitation and microemulsion method are denoted by CPO-CeO₂-ZrO₂ and MEO-CeO₂-ZrO₂, respectively. The cerium-zirconium hydroxide was also prepared by adding an ammonium hydroxide solution to a solution mixture of cerium nitrate and zirconyl nitrate. The mixing ratio of Ce:Zr was also adjusted from 4:6 to 5:5. CeO₂-ZrO₂ samples were obtained by calcining these hydroxides at 1173 K in air for 5 h. This sample is denoted by calcined CeO₂-ZrO₂ hereafter. In addition, a reduction/oxidation sample was also prepared almost according to the procedure described elsewhere [71]. The calcined CeO₂-ZrO₂ powders were heated in a flow of H₂(1%) in Ar (25 mL min⁻¹) at 1273 K for 5 h, and the obtained powders were reoxidized in oxygen flow (25 mL min⁻¹) at 873 K for 5 h. This sample is denoted by reduced/reoxidized CeO₂-ZrO₂ hereafter. The reduction behavior of the CPO- and MEO-CeO₂-ZrO₂ samples were compared with those of the calcined and reduced/reoxidized CeO₂-ZrO₂.

4.2.3. Instruments and Characterization

The composition of the CeO₂-ZrO₂ was identified by an X-ray fluorescent spectrometer (Rigaku System 3270A). The prepared particles were characterized by BET specific surface area, XRD, and temperature programmed reduction (TPR). TPR experiments of the powders were carried out in a conventional gas chromatograph equipped with a thermal conductivity detector. The reduction was carried out in a flow of H₂ (60 mL min⁻¹) using a heating rate of 10 K min⁻¹. The

reduction was carried out up to 1173 K, and the amount of H₂ uptake in the TPR was estimated from integrated peak areas.

4.3. Results and Discussion

Before presenting and discussing the results, it is useful to present the essential features of the CeO₂-ZrO₂ system. Below 1273 K, the phase diagram shows a single-phase region of monoclinic symmetry for CeO₂ molar contents less than 20%, while for CeO₂ contents higher than 80% cubic phase was reported [63, 64]. In the intermediate region, the true nature of the CeO₂-ZrO₂ phase diagram is still matter of debate [65] due to the presence of many stable and metastable phases of tetragonal symmetry [63 - 66]. According to recent investigations, three different *t*, *t'*, and *t''* phase can be distinguished on the basis of XRD and Raman characterization [65, 67, 68]. The characteristics of all the phases were summarized by Fornasiero and co-workers [58], as cited in Table 4.1. The *t* phase is a stable one formed through a diffusional phase decomposition, the *t'* phase was is obtained through a diffusionless transition and it is metastable, and the *t''* phase is generally referred to as a cubic phase because its XRD pattern is indexed in the cubic Fm3m space group. This is due to the fact that the XRD pattern is generated essentially by the cation sublattice.

Table 4.1. Classification of the phases in the CeO₂-ZrO₂ binary system [58]

Phase	Composition range (% mol Ce)	Tetragrality ^a	Space group
Monoclinic (<i>m</i>)	0-20	—	P2 ₁ /C
Tetragonal (<i>t</i>)	20-40	>1	P4 ₂ /nmc
Tetragonal (<i>t'</i>)	40-65	>1	P4 ₂ /nmc
Tetragonal (<i>t''</i>)	65-80	1	P4 ₂ /nmc
Cubic (<i>c</i>)	80-100	1	P4 ₂ /nmc

^a Defined as axial ratio *c/a*.

4.3.1. Characterization of CeO₂-ZrO₂

The sample composition of the CeO₂-ZrO₂ samples were determined by an X-ray fluorescent

Table 4.2. Composition and BET surface area data for the CeO₂-ZrO₂

Sample	Ce : Zr	Phase	BET surface area / m ² g ⁻¹	Relative amount of desorbed O ₂ ^a
CPO-CeO ₂ -ZrO ₂	4.5 : 5.5	Cubic (Pyrochlore-type)	4	1.5
MEO-CeO ₂ -ZrO ₂	3.7 : 6.3	Cubic (Pyrochlore-type)	8	1.7
Calcined CeO ₂ -ZrO ₂	4.5 : 5.5	Tetragonal	23	0.8
Reduction/reoxidation CPO-CeO ₂ -ZrO ₂	4.5 : 5.5	Cubic (Pyrochlore-type)	20	1.0

^a The peak area of reduced/reoxidized sample is regarded as 1.0

spectrometer, and the data are summarized in Table 4.2 with BET specific surface area. The composition of the MEO-CeO₂-ZrO₂ sample was controlled to become zirconium rich because the phase separation took place if the mixing ratio of Ce:Zr was adjusted from 4.6 to 5:5. The BET surface area values of the samples prepared from oxalate were smaller than those of prepared from hydroxide. The color of the samples obtained from the thermal decomposition of oxalate in argon atmosphere was black, but it changed to light yellow after the oxidation in air.

Figure 4.1 shows the XRD pattern of the CPO-CeO₂-ZrO₂ (Ce:Zr = 4.5:5.5) powders prepared by from the thermal decomposition of coprecipitated oxalate in argon flow (Fig. 4.1(a)) and oxidized in air after the decomposition (Fig. 4.1(b)). Similar results were also observed in the MEO-CeO₂-ZrO₂ sample. Both of the XRD patterns in Figure 4.1 are indexed in a Fd3m space group, indicating that the cubic phase is produced. In addition, the peaks at about 37° and 45° in the XRD patterns are the features usually observed in a cubic pyrochlore type structure. This is an interesting point since the pervious investigation reported that the oxygen mobility and desorption were strongly favored in the cubic pyrochlore structure compared to tetragonal one [56, 71].

It was also revealed that the oxidation process induce an contraction of the lattice because all the peaks in Fig. 4.1(b) shifted higher angle than those in Fig. 4.1(a). The redox processes in the solid solution are associated with the Ce³⁺/Ce⁴⁺ couple and the contraction of the lattice is therefore associated with oxidation from Ce³⁺ (0.11 nm) to Ce⁴⁺ (0.097 nm). From these results, it is suggested that the samples just prepared from the decomposition of oxalate were highly reduced

oxides, and they were oxidized upon heating at 673 K in air.

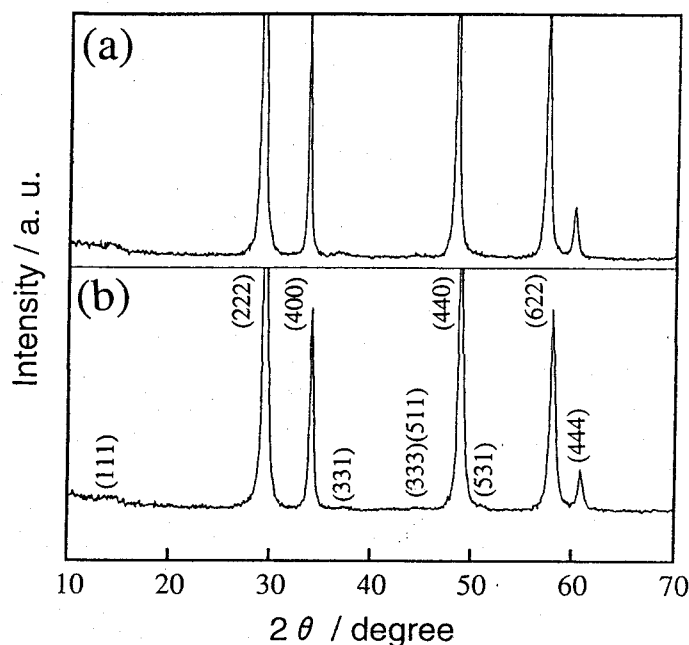


Figure 4.1. XRD patterns for $\text{CeO}_2\text{-ZrO}_2$ powders prepared from oxalate ($\text{Ce}:\text{Zr} = 4.5:5.5$): (a); starting powders heated at 1273 K for 5 h in Ar flow, (b); the sample (a) after heating in air for 2 h.

4.3.2. Reduction Behavior of $\text{CeO}_2\text{-ZrO}_2$

The reduction behavior of the $\text{CeO}_2\text{-ZrO}_2$ and effects of preparation process from oxalate or hydroxides on the TPR profiles are compared in Fig. 4.2. The TPR profiles of the $\text{CeO}_2\text{-ZrO}_2$ samples prepared from oxalate showed two peaks centered at 773 and 893-903 K, respectively. Although the peak temperatures of them slightly higher than those of the reduced/reoxidized $\text{CeO}_2\text{-ZrO}_2$, the amounts of oxygen released from the $\text{CeO}_2\text{-ZrO}_2$ samples prepared from oxalate were larger than those from the calcined and reduced/reoxidized ones in the temperature region between 573 and 973 K. The amount of H_2 uptake in the TPR which corresponds to oxygen evolution was estimated from integrated peak area. The relative amount of the desorbed oxygen is also summarized in Table 4.2, when the peak area of reduced/reoxidized sample is regarded as unit. The amounts of desorbed oxygen from the CPO- and MEO- $\text{CeO}_2\text{-ZrO}_2$ samples were 1.5 and 1.7 times, respectively, compared with that from the reduced/reoxidized one. These results clearly

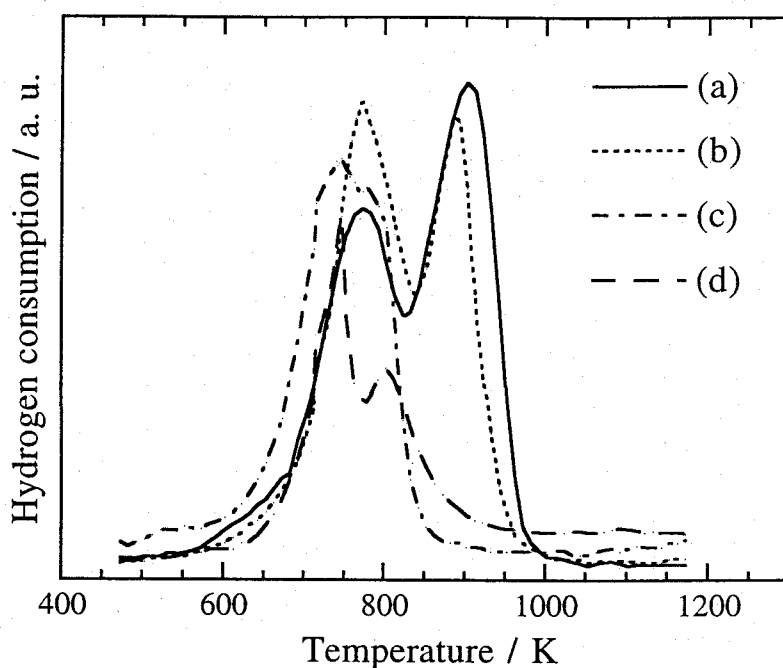


Figure 4.2. TPR profile of $\text{CeO}_2\text{-ZrO}_2$ powders: (a); Ce:Zr=3.7:6.3 prepared from the oxalate by the microemulsion method, (b); Ce:Zr=4.5:5.5 prepared from the oxalate by the coprecipitation method, (c); Ce:Zr=4.5:5.5 calcined at 1173 K in air for 5 h followed by the reduction at 1273 K for 5 h in H_2 and the reoxidation at 873 K in O_2 for 5 h, (d); Ce:Zr=4.5:5.5 calcined at 1273 K in air for 5 h.

show that the samples prepared from oxalate have high oxygen evolution property than those prepared from hydroxide.

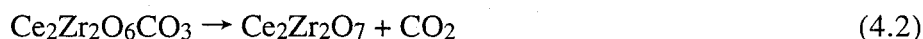
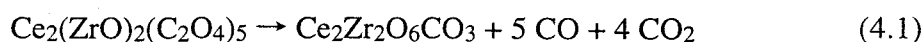
It is generally accepted that the low temperature process accounted for reduction of the surface. Because the calcined and reduced/reoxidized $\text{CeO}_2\text{-ZrO}_2$ have larger surface areas than the CPO- and MEO- $\text{CeO}_2\text{-ZrO}_2$, the reduction peak is lower by about 25 K. It has been also reported that the progressive decrease of the surface area lead to the decrease of the peak at low temperature region in the case of the redox cycled $\text{Ce}_{0.5}\text{Zr}_{0.5}\text{O}_2$ [57, 58]. The two peaks observed at 773 and 893-903 K in the samples prepared from oxalate were therefore attributed to reduction processes occurring in the bulk of the solid solution.

At present, some points appear evident from above results. The overall picture strongly suggests that the structural modifications due to addition of ZrO_2 to the CeO_2 lattice are responsible for the unusual promotion of the reduction in the bulk of the $\text{CeO}_2\text{-ZrO}_2$ solid solutions. The responsibility for the different reduction behavior in the $\text{Ce}_{0.5}\text{Zr}_{0.5}\text{O}_2$ can be explained from the

structural point of view.

As described at Section 4.1, the reason for the results that oxygen evolution behavior of the reduced and reoxidized CeO₂-ZrO₂ powders showed an unusual improvement of the reduction behavior than the only calcined samples was explained on the basis of the appearance of a new cubic phase with a pyrochlore-like structure. This new phase was formed by way of pyrochlore Ce₂Zr₂O₇ solid solution which had cubic structure with regular oxygen vacancies in the lattice. The cubic structure was remained even after the reoxidation, and as a result, the oxygen inserted in the lattice was unstable and the oxygen mobility and desorption are strongly favored compared to stable tetragonal one [56, 71]. Therefore, the oxygen evolution behavior was the best in the composition range of ZrO₂: 45 - 65 mol% that the pyrochlore-like phase efficiently appeared.

In the case of this study, the preparation process also contributed to the unusual promotion of the reduction. Taking into account of the thermal decomposition of neodymium zirconyl oxalate [72], following tentative scheme is proposed for the thermal decomposition of cerium zirconyl oxalate.



In addition, end products of the decomposition in argon flow showed a black color, suggesting the deposition of finely divided carbon particles, and the same behavior was observed in the case of the thermal decomposition of neodymium oxalate in He atmosphere [73]. According to the reference on neodymium oxalate, it can be proposed that the carbon particles are formed by the disproportion of primarily evolved CO gas during the thermal decomposition of Ce₂(ZrO)₂O₃(CO₃)₂ to Ce₂Zr₂O₆CO₃.

Moreover, the Gibbs free energy at 1273 K for the reduction of CeO₂ to Ce₂O₃ by carbon was lower than those by hydrogen and carbon monoxide [74]. All the results described above suggest that the reduction of CeO₂-ZrO₂ would be easier to produce pyrochlore Ce₂Zr₂O₇ solid solution. This would be the responsibility why the CeO₂-ZrO₂ samples prepared from oxalate have high oxygen evolution property than those prepared by way of the reduction process using hydrogen.

4.4. Conclusions

CeO₂-ZrO₂ powders with pyrochlore-like structure were prepared by means of the thermal decomposition of cerium zirconyl oxalate, and the CeO₂-ZrO₂ samples showed an excellent reduction behavior at low temperature, instead of their very low surface areas. From these results it is concluded that properly designed structural modification of the CeO₂ may lead to floating oxygens in the lattice which effectively enhance the redox properties of these catalytically interesting materials.

The amount of oxygen desorbed from the CeO₂-ZrO₂ solid solution depended on sample preparation method, and the powders prepared from the thermal decomposition of oxalate following oxidation showed more oxygen evolution than those prepared by the another methods previously reported. Therefore, the CeO₂-ZrO₂ powders prepared from oxalate possesses a excellent property as a promoter for automotive exhaust catalysts, and may be durable at high temperatures.

Summary

Chapter 1.

Cerium(IV) oxide ultrafine particles were prepared using the thermal relaxation technique called as a relaxative auto-dispersion, RAD, process. The ultrafine particles obtained were characterized by high-resolution electron microscope (HREM) observations and ultraviolet-visible spectra's measurements. HREM micrographs revealed that cerium oxide ultrafine particles were uniformly dispersed and individually isolated in the matrix. The mean particle size obtained in this process were 4.1 and 5.8 nm. Selected-area electron diffraction patterns of the particles were completely indexed as those of cerium(IV) oxide with cubic fluorite structure, and the lattice constant calculated from the radii of Debye-Sherrer rings was 5.41 Å. Bandgap energy of the ultrafine particles in the composite film was compared with that of the bulk material. However, there were no size quantization effects on the absorption edge of CeO₂.

Chapter 2.

Cerium(IV) oxide ultrafine particles were prepared using a reaction within reversed micelles, which was known as a microemulsion method. The ultrafine particles, which were obtained by mixing the W/O microemulsions containing cerium nitrate solution with those of ammonium hydroxide, were characterized by high-resolution electron microscope (HREM) observations. HREM micrographs revealed that nanometer sized CeO₂ particles were prepared and their shapes were uniform. Selected-area electron diffraction patterns of the particles were completely indexed as those of cerium(IV) oxide with the cubic fluorite structure, and the lattice constant calculated from radii of Debye-Sherrer rings was 0.541 nm. Most of the particles were distributed between 2 and 6 nm, and the mean particle size obtained in this method was between 2.6 and 4.1 nm. The size of 2.6 nm is the smallest among the values ever reported for CeO₂ particles. Both direct and indirect optical energy gaps of the particles were independent of the mean particle size, and their values were almost the same as bulk material, suggesting that there was no quantum-size effect of the CeO₂ ultrafine particles. However, the alumina-supported ultrafine CeO₂ catalysts prepared by

a microemulsion method showed much higher CO oxidation activities than those prepared by a coprecipitation method.

Chapter 3.

Nanosize ceria-zirconia ultrafine particles were prepared by the microemulsion method at $R_w=15$. HREM micrographs revealed that nanometer-sized particles were prepared and the shapes of them were uniform. The as-prepared particles were amorphous and the specific surface area of them was very large. The particle size distributed between 2 and 11 nm, and the mean particle size obtained in this method was evaluated to be 4 nm. The CO oxidation activity of the $Ce_{0.2}Zr_{0.8}O_2$ ultrafine particles impregnated on γ - Al_2O_3 powders was compared with that of the catalyst with the same composition prepared by the coprecipitation method. Both before and after the calcination in air at 1273 K for 5 h, the catalyst prepared by the microemulsion method showed higher activity. From the XRD and TEM observation, the reason for the high activity attributed to the small size and thermal stability of the particles. These results suggested that the microemulsion method was useful to synthesize the catalysts with high activity and high heat resistance.

Chapter 4.

CeO_2 - ZrO_2 solid solutions were prepared by means of the thermal decomposition of cerium zirconyl oxalate in argon flow and following oxidation in air. The reduction behavior of the obtained CeO_2 - ZrO_2 powders were investigated and compared with the samples prepared by the other methods already reported to obtain CeO_2 - ZrO_2 powders with high redox property. The CeO_2 - ZrO_2 samples prepared from oxalate showed an excellent reduction behavior, instead of their very low surface areas. The reason for the excellent oxygen evolution behavior of the powders was discussed from the viewpoints both of structure and preparation process, and it was attributed to both the appearance of a new cubic phase with a pyrochlore-like structure and the reduction by carbon formed in sample preparations.

References

- [1] R. P. Andres, R. S. Averback, W. L. Brown, L. E. Brus, W. A. Goddard, III, A. Kaldor, S. G. Louie, M. Moscovits, P. S. Peercy, S. J. Riley, R. W. Siegel, F. Spaepen and Y. Wang, *J. Mater. Res.*, **4**, 704 (1989).
- [2] A. Tschöpe and J. Y. Ying, *NanoStructured Materials*, **4**, 617 (1994).
- [3] F. Imoto, T. Nanataki and S. Kaneko, *Ceram. Trans.*, **1**, 204, (1988).
- [4] P. L. Chen and I. W. Chen, *J. Am. Ceram. Soc.*, **76**, 1577 (1993).
- [5] W. P. Hsu, L. Rönquist and E. Matijevic, *Langmuir*, **4**, 31 (1988).
- [6] Y. C. Zhou and M. N. Rahaman, *J. Mater. Res.*, **8**, 1680 (1993).
- [7] M. Hirano and E. Kato, *J. Am. Ceram. Soc.*, **79**, 777 (1996).
- [8] W. Chebgyun, Q. Yitai, W. Changsui, Y. Li and Z. Guiwen, *Mat. Sci. Eng.*, **B39**, 160 (1996).
- [9] Y. Zhou, R. J. Phillips and J. A. Switzer, *J. Am. Ceram. Soc.*, **78**, 981 (1995).
- [10] E. Kay and M. Hecq, *J. App. Phys.*, **55**, 370 (1984).
- [11] R. A. Roy, R. Messier and S. V. Krishnaswamy, *Thin Solid Films*, **109**, 27 (1983).
- [12] Y. Asano, *Thin Solid Films*, **105**, 1 (1983).
- [13] L. Martinu, H. Biederman and J. Zemek, *Vacuum*, **35**, 171 (1985).
- [14] K. Kashiwagi, Y. Yoshida and Y. Murayama, *J. Vac. Sci. Technol. A*, **5**, 1828 (1987).
- [15] L. Martinu, *Thin Solid Films*, **140**, 307 (1986).
- [16] J. Perrin, B. Despax and E. Kay, *Phys. Rev. B*, **32**, 719 (1985).
- [17] T. Noguchi, K. Gotoh, Y. Yamaguchi and S. Deki, *J. Mater. Sci. Lett.*, **10**, 477 (1991).
- [18] P. L. Pileni, ed. *Structure and Reactivity in Reverse Micelles*, Elsevier, (1989).
- [19] M. Ueda and Z. A. Schelly, *Langmuir*, **4**, 653 (1988).
- [20] T. Kawai, K. Hamada, N. Shindo and K. Kon-no, *Bull. Chem. Soc. Jpn.*, **65**, 2715 (1992).
- [21] A. J. W. G. Visser, K. Vos, A. van Hoek and J. S. Santema, *J. Phys. Chem.*, **92**, 759 (1988).

- [22] H. F. Eicke, J. C. W. Shepherd and A. Sternemann, *J. Colloid Interface Sci.*, **56**, 168 (1976).
- [23] S. S. Atic and J. K. Thomas, *J. Am. Chem. Soc.*, **103**, 3543 (1981).
- [24] P. D. I. Fletcher, A. M. Howe and B. H. Robinson, *J. Chem. Soc. Faraday Trans. I*, **83**, 985 (1987).
- [25] J. Lang, A. Jada and A. Malliaris, *J. Phys. Chem.*, **92**, 1946 (1988).
- [26] M. A. López-Quintela and J. Rivas, *J. Colloid Interface Sci.*, **158**, 446 (1993).
- [27] T. Noguchi, K. Goto, Y. Yamaguchi and S. Deki, *J. Mater. Sci. Lett.*, **11**, 648 (1992).
- [28] T. Noguchi, S. Murakami, K. Gotoh, Y. Yamaguchi and S. Deki, *J. Mater. Sci. Lett.*, **11**, 797 (1992).
- [29] Y. Yamaguchi, T. Noguchi, K. Gotoh and S. Deki, *Sen-i Gakkaishi*, **49**, 124 (1993).
- [30] K. Gotoh, T. Noguchi, S. Murakami, Y. Yamaguchi and S. Deki, *Koubunshi Ronbunshu*, **50**, 437 (1993).
- [31] The file of X-ray powder diffraction standards by the American Society for the Testing and Materials. Inorganic compounds : CeO₂, 34-394.
- [32] N. Serpone, D. Lawless and R. Khairutdinov, *J. Phys. Chem.*, **99** 16646 (1995).
- [33] R. A. Van Leeuwen, C.-J. Hung, D. R. Kammler and J. A. Switzer, *J. Phys. Chem.*, **99**, 15247 (1995).
- [34] K. B. Sundaram and P. Wahid, *Phys. Stat. Sol. B*, **161**, K63 (1990).
- [35] Z. C. Orel and B. Orel, *Phys. Stat. Sol. B*, **186**, K33 (1994).
- [36] M. Boutonnet, J. Kizling, P. Stenius and G. Maire, *Colloids and Surfaces*, **5**, 209 (1982).
- [37] C. Petit, *J. Phys. Chem.*, **97**, 6961 (1993).
- [38] C. Petit, P. Lixon and M. P. Pileni, *J. Phys. Chem.*, **97**, 12974 (1993).
- [39] M. P. Pileni and I. Lisiecki, *Colloids and Surfaces*, **80**, 63 (1993).
- [40] M. Gobe, K. Kon-no, K. Kandori and A. Kitahara, *J. Colloid Interface Sci.*, **93**, 293 (1983).
- [41] S. D. Ramamurthi, Z. Xu and D. A. Payne, *J. Am. Ceram. Soc.*, **73**, 2760 (1990).
- [42] T. Sano, T. Kawai and K. Kon-no, *Proceedings of the International Conference on Color*

Materials, Osaka, p. 120, (1992).

- [43] P. F. Zinsli, *J. Phys. Chem.*, **83**, 3223 (1979).
- [44] C. A. Hogarth and Z. T. Al-Dhhan, *Phys. Stat. Sol. B*, **137**, K157 (1986).
- [45] Z. C. Orel and B. Orel, *Sol. Energy Mater. Sol. Cells.*, **40**, 205 (1996).
- [46] H. Yao and Y. F. Yu-Yao, *J. Catal.*, **86**, 254 (1984).
- [47] M. Haneda, T. Mizushima, N. Kakuta, A. Ueno, Y. Sato, S. Matsuura, K. Kasahara and M. Sato, *Bull. Chem. Soc. Jpn.*, **66**, 1279 (1993).
- [48] A. Tschöpe, W. Liu, M. Flytzani-Stephanopoulos and J. Y. Ying, *J. Catal.*, **157**, 42 (1995).
- [49] K. C. Taylor, Automobile catalytic converters. In *Catalysis - Science and technology*; Eds, J. R. Anderson and M. Boudert., Springer - Verlag: Berlin, Vol. 5 (1984).
- [50] D. M. J. Bevan, *J. Inorg. Nucl. Chem.*, **1**, 49 (1955).
- [51] M. Ozawa, M. Kimura, H. Sobukawa and K. Yokota, *Toyota Technical Review*, **27**, 43 (1992).
- [52] K. J. Blackenburg and A. K. Datye, *J. Catal.*, **128**, 1 (1991).
- [53] B. Harrison, A. F. Dwiwell and C. Hallet, *Plat. Met. Rev.*, **32**, 73 (1988).
- [54] M. Ozawa, M. Kimura and A. Isogai, *J. Alloys and Compounds*, **193**, 73 (1993).
- [55] T. Murota, T. Hasegawa, S. Aozasa, H. Matsui and M. Motoyama, *J. Alloys and Compounds*, **193**, 298 (1993).
- [56] P. Fornasiero, R. D. Monte, G. R. Rao, J. Kaspar, S. Meriani, A. Trovarelli and M. Graziani, *J. Catal.*, **151**, 168 (1995).
- [57] G. Balducci, P. Fornasiero, R. Di Monte, J. Kaspar, S. Meriani and M. Graziani, *Catal. Lett.*, **33**, 193 (1995).
- [58] P. Fornasiero, G. Balducci, R. D. Monte, J. Kaspar, V. Sergo, G. Gubitosa, A. Ferrero and M. Graziani, *J. Catal.*, **164**, 173 (1996).
- [59] M. H. Yao, R. J. Baird, F. W. Kunz and T. E. Hoost, *J. Catal.*, **166**, 67 (1997).
- [60] G. R. Rao, P. Fornasiero, R. D. Monte, J. Kaspar, G. Vlaic, G. Balducci, S. Meriani, G. Gubitosa, A. Cremona and M. Graziani, *J. Catal.*, **162**, 1 (1996).

- [61] M. Kishida, T. Fujita, K. Umakoshi, J. Ishiyama, H. Nagata and K. Wakabayashi, *J. Chem. Soc., Chem. Commun.*, **1995**, 763.
- [62] M. Kishida, K. Umakoshi, J. Ishiyama, H. Nagata and K. Wakabayashi, *Catal. Today*, **29**, 355 (1996).
- [63] E. Tani, M. Yoshimura and S. Somiya, *J. Am. Ceram. Soc.*, **66**, 506 (1983).
- [64] P. Duran, M. Gonzalez, C. Moure, J. R. Jurdo and C. Pascal, *J. Mater. Sci.*, **25**, 5001 (1990).
- [65] M. Yashima, K. Morimoto, N. Ishizawa and M. Yoshimura, *J. Am. Ceram. Soc.*, **76**, 1745 (1993).
- [66] S. Meriani, *Mat. Sci. Eng.*, **A109**, 121 (1990).
- [67] M. Yashima, K. Morimoto, N. Ishizawa and M. Yoshimura, *J. Am. Ceram. Soc.*, **76**, 2865 (1993).
- [68] M. Yashima, H. Arashi, M. Kakihana and M. Yoshimura, *J. Am. Ceram. Soc.*, **77**, 1067 (1994).
- [69] S. Meriani, *Mat. Sci. Eng.*, **71**, 369 (1985).
- [70] S. Meriani and G. Spinolo, *Powder Diffr.*, **2**, 255 (1987).
- [71] S. Otsuka-Yao, H. Morikawa, N. Izu and K. Okuda, *Nippon Kinzoku Gakkaishi*, **12**, 1237 (1995).
- [72] V. B. Reddy and P. N. Mehrotra, *J. Thermal Anal.*, **29**, 399 (1984).
- [73] Y. Saito and S. Sasaki, *Report of the Reseach Laboratory of Engineering Materials, Tokyo Institute of Technology*, **6**, 69 (1981).
- [74] Gmelin Handbuch der Anorganischen Chemie, System Nr. 39, Sc, Y, La und Lanthanide - Seltenerdelemente, Teil C1, Hydride; Oxide, Springer-Verlag, Berlin, 1974.

Acknowledgments

The author would like to express his heartfelt gratitude to Professor Dr. Gin-ya Adachi, Department of Applied Chemistry, Faculty of Engineering, Osaka University, for his continuous guidance, many invaluable suggestions, and his sincere encouragement throughout this work. The author would also like to thank Professor Dr. Yasuhiko Shirota and Professor Dr. Toshikazu Hirao, Department of Applied Chemistry, Faculty of Engineering, Osaka University for their helpful comments and suggestions.

The author is indebted to Associate Professor Dr. Ken-ichi Machida for his constant guidance and stimulating discussions, and Dr. Nobuhito Imanaka and Dr. Hiroki Sakaguchi for their valuable suggestions and heartfelt advices.

The author makes grateful acknowledgement to Professor Dr. Hirotaro Mori and Dr. Takao Sakata, Research Center for Ultra-High Voltage Electron Microscopy, Osaka University for their collaborations and useful discussion.

The author desires to express his sincere thanks to Associate Professor Dr. Noritetsu Yoshida, Faculty of Science, Kobe University for his helpful comments and assistance in measuring temperature-programmed-reduction spectra.

Furthermore, the author is much obliged to Professor Dr. Masao Nasu, Dr. Katsuji Tani, and Mr. Akifumi Murase, Department of Pharmacy, Faculty of Pharmaceutical Sciences, Osaka University for their assistance in centrifuging of the ultrafine particles.

The author also thanks to Shin-Nippon Kinzoku Kagaku Co.,Ltd. for supplying starting materials.

Special thanks should be given to the author's co-workers, Mr. Kazuyasu Fujiwara, Mr. Yumin Peng, and Mr. Atsushi Obayashi for their helpful assistance and support in the course of this work, and all other members of the research group under direction of Professor G. Adachi, Osaka University.

The Japan Society for the Promotion of Science is also acknowledged for a research fellowship.

Finally, the author is particularly grateful to his beloved parents the late Mr. Sumio Masui and Mrs. Keiko Masui, and his brother Mr. Yoshinari Masui for their perpetual support and hearty encouragement.